Multidecadal ozone trends in China and implications for human health and crop yields: A hybrid approach combining chemical transport model and machine learning

Jia Mao[1], Amos P. K. Tai[1,2,3], David H. Y. Yung[1], Tiangang Yuan[1], Kong T. Chau[1], and Zhaozhong Feng[3,4]

[1] Earth and Environmental Sciences Programme and Graduate Division of Earth and Atmospheric Sciences, Faculty of Science, The Chinese University of Hong Kong, Hong Kong SAR, China

[2] State Key Laboratory of Agrobiotechnology, and Institute of Environment, Energy and Sustainability, The Chinese University of Hong Kong, Hong Kong SAR, China

[3] Collaborative Innovation Center on Forecast and Evaluation of Meteorological Disasters (CIC-FEMD), Nanjing University of Information Science and Technology, Nanjing, Jiangsu, China

[4] Key Laboratory of Ecosystem Carbon Source and Sink, China Meteorological Administration (ECSS-CMA), Nanjing University of Information Science & Technology, Nanjing, Jiangsu, China

Correspondence to: Amos P. K. Tai (amostai@cuhk.edu.hk)

Abstract. Surface ozone (O_3) is well known to pose significant threats to both human health and crop production worldwide. However, a multi-decadal assessment of O_3 impacts on public health and crop yields in China is lacking due to insufficient long-term continuous O_3 observations. In this study, we used a machine learning (ML) algorithm to correct the biases of O_3 concentrations simulated by the chemical transport model from 1981–2019 by integrating multi-source datasets. The ML-enabled bias correction offers improved performance in reproducing observed O_3 concentrations, and thus further improves our estimates of O_3 impacts on human health and crop yields. The warm-season increasing trend of O_3 in Beijing-Tianjin-Hebei and its surroundings (BTHs), Yangtze River Delta (YRD), Sichuan Basin (SCB) and Pearl River Delta (PRD) regions are 0 .32 μg m^{-3} yr^{-1}, 0.63 μg m^{-3} yr^{-1}, 0.84 μg m^{-3} yr^{-1}, and 0.81 μg m^{-3} yr^{-1} from 1981 to 2019, respectively. In more recent years, O_3 concentrations experience more fluctuations in the four major regions. Our results show that only BTHs have a perceptible increasing trend of 0.81 μg m^{-3} yr^{-1} during 2013–2019. Using AOT40-China exposure-yield response relationships, the estimated relative yield losses (RYLs) for wheat, rice, soybean and maize are 17.6%, 13.8%, 11.3% and 7.3% in 1981, and increases to 24.2%, 17.5%, 16.3% and 9.8% in 2019, with an increasing rate of +0.03% yr^{-1}, +0.04% yr^{-1}, +0.27% yr^{-1} and +0.13% yr^{-1}, respectively. The estimated annual all-cause premature deaths induced by O_3 increase from ~55,900 in 1981 to ~162,000 in 2019 with an increasing trend of ~2,980 deaths yr^{-1}. The annual premature deaths related to respiratory and cardiovascular disease are ~34,200 and ~40,300 in 1998, and ~26,500 and ~79,000 in 2019, having a rate of change of −546 and +1,770 deaths yr^{-1} during 1998–2019, respectively. Our study, for the first time, used ML to provide a robust dataset of O_3 concentrations over the past four decades in China, enabling a long-term evaluation of O_3-induced crop losses and health impacts. These findings are expected to fill the gap of the long-term O_3 trend and impact assessment in China.

1 Introduction

Surface ozone (O_3), an important secondary air pollutant, is mainly generated through photochemical reaction of volatile organic compounds (VOCs), carbon monoxide (CO), and nitrogen oxides (NO$_x$) in the presence of sunlight. As a strong oxidant, O_3 at the ground level is detrimental to human health and vegetation. More recently, due to the rapid

urbanization and industrialization, the summertime O_3 pollution has become an emerging concern in China. Li et al. (2020) reported that the mean summer 2013–2019 trend in maximum daily 8-h average surface O_3 (MDA8-O_3) was +1.9 ppb yr^{-1} in China, with high values widely observed in the North China Plain (NCP), Yangtze River Delta (YRD), and Pearl River Delta (PRD) regions. On the regional scale, the exposure of humans and vegetation to O_3 is greater in China than in other developed regions of the world (Lu et al., 2018). Several studies have suggested the important roles of climate and land cover changes on O_3 pollution in addition to anthropogenic emissions (Fu and Tai, 2015; Wang et al., 2020). It has been suggested that global warming and the changing land use may further increase surface O_3 by the late 21st century (Kawase et al., 2011; Wang et al., 2020), which can pose greater threats to human health and food security.

Meteorological factors can modulate the temporal and spatial patterns of O_3 via affecting the physical and chemical processes within the atmosphere (Liu et al., 2019; Mao et al., 2020; Yin and Ma, 2020). High temperature, low relative humidity and low planetary boundary height are conducive to the photochemical production and O_3 accumulation. Jacob and Winner (2009) summarized that the enhanced O_3 levels at higher temperatures are primarily driven by increased biogenic VOC emissions from vegetation and reduced lifetimes of peroxyacetyl nitrate (PAN) due to accelerated decomposition of PAN into NO_x. Besides, the changes in wind speed and direction can affect O_3 concentrations through transport. Land cover and land use change affects O_3 air quality by perturbing surface fluxes, hydrometeorology, and concentrations of atmospheric chemical components (Tai et al., 2013; Fu and Tai, 2015; Liu et al., 2020; Ma et al., 2021). For instance, the terrestrial biosphere is a major source of isoprene, which plays a significant role in modulating O_3 concentrations. In the Intergovernmental Panel on Climate Change (IPCC) A1B scenario, Tai et al. (2013) found that widespread crop expansion could reduce isoprene emission by ∼10 % globally compared with the present land use. Such a reduction could decrease O_3 by up to 4 ppb in the eastern US and increase O_3 by up to 6 ppb in South and Southeast Asia, whereby the difference in the sign of responses is primarily determined by the different O_3 production regimes.

The increasing health burden due to air pollution has become an important contributor to global disease burden. Some recent studies have demonstrated that short-term O_3 exposure negatively impacts human health, especially via respiratory, and cardiovascular mortality (Shang et al., 2013; Yin et al., 2017b; Feng et al., 2019; Zhang et al., 2022a). In 2015–2018, the estimated annual total premature mortality related to O_3 pollution in 334 Chinese cities was 0.27 million for 2015, 0.28 million for 2016, 0.39 million for 2017, and 0.32 million for 2018 (Zhang et al., 2021). Maji and Namdeo (2021) reported that short-term all-cause, cardiovascular and respiratory premature mortalities attributed to the ambient 4th highest MDA8-O_3 exposure were 156,000, 73,500 and 28,600 in 2019, showing increases of 19.6%, 19.8% and 21.2%, respectively, compared to 2015. Zhang et al. (2022b) reported that each 10 μg m^{-3} increase in the MDA8-O_3 can lead to a rise of 0.41 % (95 % CI: 0.35 %–0.48 %) in all-cause, 0.60 % (95 % CI: 0.51 %– 0.68 %) in cardiovascular and 0.45 % (95 % CI: 0.28 %– 0.62 %) in respiratory mortality.

The damage to plants induced by O_3 is mainly caused by the stomatal uptake of O_3 into the leaf interior instead of direct plant surface deposition (e.g., Clifton et al., 2020). In previous studies, a variety of concentration-based metrics have been widely used to assess the O_3 risks to crop yield and ecosystem functions. Initially, a 7-hour (09:00–15:59) mean metric (M7) was proposed, which was later extended to a 12-hour (08:00–19:59; referred to M12) to include late-day O_3 concentrations. Cumulative metrics have also been developed to evaluate the impacts of O_3 on crops. The accumulated O_3 over a threshold of 40 ppb (AOT40) is a widely used metric to evaluate the phytotoxic effects of O_3. Compared to AOT40 using a linear function, another metrics, W126, considers the nonlinear response of yield loss to O_3 exposure whereby higher O_3 concentrations will progressively induce more severe yield losses. However, many studies have suggested that the stomatal uptake of O_3 is more related to vegetation damage than O_3 exposure per se (Feng et al., 2012; Feng et al., 2018; Pleijel et al., 2022). In the recent two decades, the flux-based approach therefore has been developed and increasingly used to assess the relationships between the stomatal O_3 uptake and crop yields. Tai et al. (2021) compared the results of the estimated global crop yield losses using three concentration-based and two flux-based O_3 exposure metrics, and showed that the concentration-based metrics differ greatly among themselves, while the two flux-based metrics are generally close

82   to each other, which lie close to the middle of the range covered by all metrics.

83   At present, a comprehensive long-term assessment of O_3 impacts is hindered by a lack of continuous O_3 observations
84   in China (Lu et al., 2018; Gong et al., 2021). From both health and food perspectives, reliable long-term estimates of O_3
85   are critically needed to better understand the O_3 damage over the past few decades since the beginning of rapid industrial
86   transformation in the 1980s. In previous studies, various alternative approaches have been used to address the problem of
87   insufficient observations. The multiple linear regression (MLR) model is often used for extrapolation to construct
88   spatiotemporal distributions of air pollutants (Moustris et al., 2012; Abdullah et al., 2017). However, the linear statistical
89   methods are generally limited by their incapability to capture the nonlinear relationships between air pollutants and
90   precursors as well as meteorological fields. Chemical transport models (CTMs), based on mathematical representation of
91   atmospheric physical and chemical processes, are also the common tool to simulate air pollutant concentrations
92   spatiotemporally (Fusco and Logan, 2003; Liu and Wang, 2020a; Wang et al., 2022a). Taking the advantages of the CTM,
93   Fu and Tai (2015) investigated the impacts of historical climate and land cover changes on tropospheric O_3 in East Asia
94   between 1980 and 2010. However, the utility of CTMs is often limited by their high computational cost when conducting
95   long-term simulations at high spatiotemporal resolutions. Large biases also exist due to uncertainties in historical emission
96   inventories, parameterization of physical and chemical processes, and initial and/or boundary conditions, and these errors
97   tend to increase at finer spatiotemporal scales.

98   In recent years, machine learning (ML) methods have gained increasing popularity in air pollution studies (Liu et al.,
99   2020; Ma et al., 2021). In the early stage of applying ML to atmospheric chemistry, ML methods were usually used as an
100   independent method from CTMs (Hu et al., 2017; Zhan et al., 2017), for instance, to predict O_3 concentrations by mapping
101   the nonlinear relationships between observed O_3 concentrations and their possible shaping factors. These applications are
102   usually purely data-driven, whereby the ML algorithms do not involve any representation of the physical mechanisms
103   behind the relevant processes. With powerful algorithms and user-friendly hyperparameter tuning processes, some well-
104   trained ML models, driven by data from multiple sources including reanalysis and satellite data, have shown even higher
105   predictive capacity than process-based models. The advantages of ML methods over CTMs include more flexible choices
106   for input data and spatiotemporal resolution, and substantially lower computational costs (Bi et al., 2022). However, purely
107   data-driven ML methods are known to suffer a lack of transparency and interpretability, which renders it more difficult to
108   offer adequate scientific interpretation for the physical mechanisms behind. Thus, a hybrid approach combining ML
109   algorithms and CTM-simulated results have been increasingly used to predict air pollutants and understand their trends in
110   recent years. Integrating data from various sources, ML methods have been used as a tool to correct the biases in the lower-
111   resolution simulated results from CTMs (Di et al., 2017; Ivatt and Evans, 2020; Ma et al., 2021). Based on process-based
112   CTMs integrating decades of accumulated knowledge in Earth system science, while taking advantage of ML to address
113   still-existing model errors, the hybrid approach has great potential in tackling air quality problems (Irrgang et al., 2021).

114   In this work, we incorporated the O_3 concentrations directly simulated by the Goddard Earth Observing System
115   coupled with Chemistry (GEOS-Chem) model at a lower resolution into a bias-corrected, finer-resolution dataset by
116   integrating them with O_3 observations from 2016 to 2018 (for validation purpose), high-resolution metetrological fields,
117   land use data and other geographical information from multiple sources using a tree-based ML algorithm, LightGBM. The
118   final high-resolution hourly O_3 dataset with a resolution of 0.25°×0.25° from 1981 to 2019 was further used to assess the
119   impacts of O_3 on human health and crop yields over the past four decades. The simultaneous analysis of the combined
120   impacts of O_3 on agriculture and human health can offer more comprehensive policy implications for the mitigation of O_3-
121   related impacts across China.

2 Data and methods

2.1 Air quality, meteorological, land and crop data

Hourly surface O_3 observations ($\mu g\ m^{-3}$) from 2016 to 2018 were obtained from the China National Environment Monitoring Center Network (http://106.37.208.233:20035/) established by the Ministry of Ecology and Environment of China. The MDA8-O_3 of each site was calculated with at least 14 valid hourly values from 08:00 to 24:00 local time. A total of 1016 sites were selected after deleting the missing and abnormal data (**Fig. 1**).
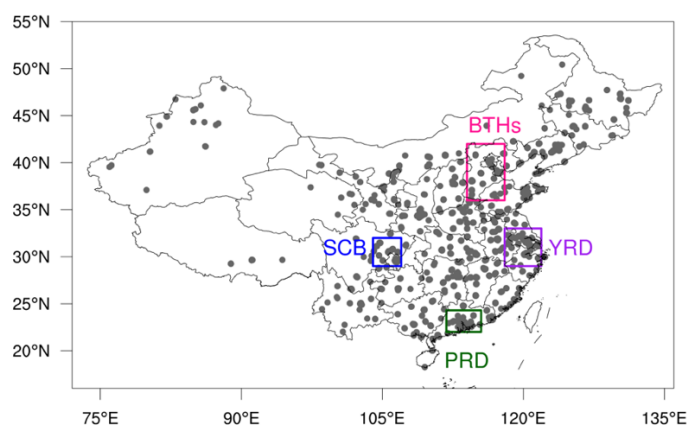
Figure 1. Study domain and locations of the selected monitoring sites. The pink, blue, purple and green rectangles indicate the Beijing-Tianjin-Hebei and its surroundings (BTHs), Sichuan Basin (SCB), Yangtze River Delta (YRD), and Pearl River Delta (PRD) regions, respectively, for more detailed analysis.

The surface meteorological fields used in this study include sea surface pressure, horizontal wind at 10 m, air temperature at 2 m, downward solar radiation, surface albedo, and total precipitation. The variables selected at 850 hPa and 100 hPa include relative humidity, horizontal and vertical velocity. These meteorological variables have been shown by many previous studies to correlate strongly with surface O_3 concentrations as discussed above. Hourly reanalysis data for meteorological variables were obtained from the fifth generation European Center for Medium-Range Weather Forecasts (ECMWF) reanalysis dataset (ERA5) with a spatial resolution of 0.25°×0.25° from 1981 to 2019 (https://cds.climate.copernicus.eu/). This spatial resolution sets the highest limit of resolution for our hybrid O_3 product.

The national land use data with a spatial resolution of 1 km×1 km for 2013 were obtained from the Resource and Environment Science Data Center of the Chinese Academy of Sciences (RESDC) (http://www.resdc.cn). Six primary types of land use are considered: cultivated land, forestland, grassland, water bodies, construction land, and unused land. Nationwide elevation data were also provided by the RESDC (https://www.resdc.cn/data.aspx?DATAID=123), which is resampled based on the latest Shuttle Radar Topography Mission (SRTM) V4.1 data developed in 2000.

The spatial distribution of the harvested areas for four staple crops (wheat, rice, maize, soybean) for China was obtained from the Global Agro-Ecological Zones 2015 dataset (https://doi.org/10.7910/DVN/KJFUO1). Crop harvesting dates with a resolution of 0.5°×0.5° were provided by the Center for Sustainability and the Global Environment (Sacks et al., 2010). For crops having more than one growing season in a year, only the primary growing period was considered.

2.2 GEOS-Chem model

We used the GEOS-Chem global 3-D chemical transport model version 12.2.0 (http://acmg.seas.harvard.edu/geos/), driven by assimilated meteorological data from Modern Era Retrospective-analysis for Research and Applications, Version 2 (MERRA2) (https://gmao.gsfc.nasa.gov/reanalysis/MERRA-2/) with a horizontal resolution of 2.0° latitude by 2.5°

152 longitude and reduced vertical resolution of 47 levels. GEOS-Chem incorporates meteorological conditions, emissions,
153 chemical information, and surface conditions to simulate the formation, transport, mixing and deposition of ambient O_3. It
154 performs fully coupled simulations of O_3-NO_x-VOC-aerosol chemistry (Bey et al., 2001). Previous studies have
155 demonstrated the ability of GEOS-Chem to reasonably reproduce the magnitudes and seasonal variations of surface O_3
156 East Asia (Wang et al., 2011; He et al., 2012). To provide long-term simulated O_3 fields for incorporation into the ML
157 model (see below), we conducted GEOS-Chem simulations at a resolution of 2.0°×2.5°; higher resolutions of GEOS-Chem
158 in nested grids are available but computationally prohibitive for multi-decadal simulations. The original unit of GEOS-
159 Chem-simulated O_3 is ppb, which was converted to $\mu g\ m^{-3}$ assuming a constant temperature of 25°C and pressure of
160 1013.25 hPa (1 $\mu g\ m^{-3}$ is approximately 0.5 ppb) when compared with observations (Yin et al., 2017b; Gong and Liao,
161 2019).

162   Global anthropogenic emissions of CO, NO_x, SO_2 and VOCs are from Community Emissions Data System (CEDS),
163 which has coverage over the simulation years of 1950–2014 (Hoesly et al., 2018). Biomass burning emissions are from the
164 GFED-4 inventory (van der Werf et al., 2017). Biogenic VOC emissions are computed by the Model of Emissions of Gases
165 and Aerosols from Nature (MEGAN) v2.1 (Guenther et al., 2012), which is embedded in GEOS-Chem. Emissions of
166 biogenic VOC species in each grid cell, including isoprene, monoterpenes, methyl butenol, sesquiterpenes, acetone and
167 various alkenes, are simulated as a function of canopy-scale emission factors modulated by environmental activity factors
168 to account for changing temperature, light, leaf age, leaf area index (LAI), soil moisture and CO_2 concentrations
169 (Sindelarova et al., 2014).

170   Dry deposition follows the resistance-in-series scheme of Wesely (1989), which depends on species properties, land
171 cover types and meteorological conditions, and uses the Olson land cover classes with 76 land types reclassified into 11
172 land types. Although transpiration is a potential mechanism via which the land cover affects ozone, we do not address it in
173 this study because water vapor concentration in GEOS-Chem is prescribed from assimilated relative humidity (i.e., not
174 computed online from evapotranspiration).

175 **2.3 LightGBM machine-learning model**

176   The primary purpose of utilizing ML here was to minimize the biases of model output as compared with observations,
177 whereby the biases could arise from incomplete model physics, input and parameter errors, numerical errors, coding errors,
178 as well as representation errors (i.e., mismatch in spatial scales between model grid cells and site observations), so that the
179 output of the hybrid model could have the closest values to the observations and enable more accurate impact evaluation.
180 In this study, we used the LightGBM ML algorithm to integrate GEOS-Chem-simulated O_3 at a lower resolution with
181 higher-resolution multi-source data to produce higher-resolution hourly O_3 and MDA8-O_3 fields.

182   LightGBM is a ML algorithm based on the gradient boosting decision tree (Chen and Guestrin, 2016), which has a
183 high training efficiency and lower memory footprint, and thus is suitable for processing massive high-dimensional data
184 (Zhang et al., 2019). The general steps to build a ML model can be summarized as follows: (1) choose an algorithm
185 appropriate for the problem (e.g., regression or classification); (2) clean the data and split them into training and test data;
186 (3) train and tune the model with training data to well capture prediction patterns; (4) evaluate model performance on test
187 data; and (5) return to step (3) and (4) until an optimal predictive ability is reached. The training and evaluation processes
188 are both performed at the site level in accordance with the observations, whereby the predictor variables and model
189 responses were first sampled at the same locations using the bilinear interpolation approach (Accadia et al., 2003). This
190 approach of handling spatial scale mismatch between model grid cells and site observations has been commonly used in
191 previous studies (e.g., Li et al., 2021). When predicting the gridded O_3 concentrations with the trained model, predictor
192 variables at different spatial resolutions were all regridded to the same resolution of 0.25°×0.25° consistent with the ERA5
193 meteorological fields. By taking the advantage of these higher-resolution datasets, the hybrid approach can not only correct

194 the biases of the GEOS-Chem-simulated O_3, but also refine them into a finer resolution. To evaluate if the hybrid approach

195 truly benefits from using a higher-resolution meteorological fields, we also repeated the whole training exercise with the

196 input meteorology of GEOS-Chem (MERRA2 at 2.0°×2.5°) instead of ERA5.

197   During the model training process, the model was evaluated with 10-fold cross-validation to ensure the robustness

198 and reliability of the model, whereby the training data were randomly partitioned into 10 subsets of approximately the same

199 size, with 90% of data used to train individual models and the ensemble model, and the remaining 10% of data used to

200 examine model performance (Xiao et al., 2018). This process was repeated 10 times so that each data record was left for

201 testing once. The tuning of the hyperparameters was optimized using grid search optimization to improve detection

202 performance and diagnostic accuracy (Wang et al., 2019). Statistical indicators, including the coefficient of determination

203 (R^2) and root-mean-square error (RMSE), were used in subsequent assessment of model performance for GEOS-Chem

204 alone and for the hybrid approach.

205   Our analysis revealed that training the model with one year or more of data results in only marginal reductions in

206 RMSE and enhancements in R^2 (**Fig. S1**); thus a timescale of two years appears to strike a good balance between

207 computational burden and model accuracy. These results align with the findings of Ivatt and Evans (2020), who suggested

208 that much of the variability in the power spectrum of surface O_3 can be captured by timescales of a year or less. Therefore,

209 here we utilized observations from the period 2016-2017 as the training data, which offered a more economical computing

210 cost and improved training time efficiency, and observations in 2018 as the independent test data to evaluate model

211 performance.

212 **2.4 Ozone exposure metric and exposure–yield response functions**

213   Among O_3 exposure indices, AOT40 has been used widely during the last two decades as it has been found to have a

214 strong relationship with relative yield of many crop species (Mills et al., 2007), and thus was used to quantify the impacts

215 of surface O_3 on crop yields in this study. The flux-based metrics, which require long-term simulations using a process-

216 based stomatal uptake model, were beyond the scope of this study. The AOT40 (ppm-h) is defined as follows:

$$AOT40 = \sum_{i=1}^{n}([O_3]_i - 0.04) \tag{1}$$

218 where the $[O_3]_i$ is the hourly mean O_3 concentration (ppm) during the 12 hours of local daytime (08:00–19:59); n is the

219 number of hours in the growing season defined as the 90 days prior to the start of the harvesting period according to the

220 crop calendar.

221   The exposure–yield response functions based on extensive field experimental studies have been established to relate

222 a quantifiable O_3-exposure metrics to crop yields. It has been suggested that responses of crop yields were found greater

223 in Asian experiments than the American and European counterparts, indicating possibly higher O_3 sensitivity of Asian crop

224 varieties (Emberson et al., 2009; Feng et al., 2022). To better understand O_3-induced risks to crops in China, the AOT40

225 exposure-yield functions developed based on field experiments in China are used in this study, which are named as AOT40-

226 China. The exposure–yield response functions for soybean is from Zhang et al. (2017), and for other three crops are from

227 Feng et al. (2022). The statistical exposure-yield relationships used in this study are summarized in **Table S1**.

228 **2.5 Analysis of health impacts**

229   All-cause mortality, cardiovascular disease mortality and respiratory disease mortality are selected as the health

230 outcomes of our study due to the high correlation between these endpoints and short-term O_3 exposure in previous studies.

231 A log-linear exposure-response function is widely adopted and recommended by the World Health Organization (WHO)

232 for health impact assessment in areas with severe air pollution. In particular, the log-linear model is the most widely applied

233 exposure-response model at present in China (Lelieveld et al., 2015; Yin et al., 2017a; Zhang et al., 2022b). The premature
234 mortality is calculated following:

$$\Delta M = \delta c * \left[\frac{(RR - 1)}{RR} \right] * P \tag{2}$$

236 where ΔM is the excess mortality attributable to O_3 exposure; δc is the baseline mortality rate for a particular health endpoint
237 (Yin et al., 2017b; Madaniyazi et al., 2016); P is the exposed population; and RR is the relative risk defined as:

$$RR = \exp((X - X_0) * \beta) \tag{3}$$

239 where β is the exposure-response coefficient derived from epidemiological cohort studies (Shang et al., 2013); X represents
240 the model-calculated O_3 concentration; the value of X_0 is the threshold concentration below which no additional risk is
241 assumed. Consistent with previous studies (Lelieveld et al., 2015; Liu et al., 2018), we used $X_0 = 75.2$ μg m^{-3}.

242   In this study, the mean MDA8-O_3 concentrations in warm season (May-September) were used to estimate the disease-
243 specific health impacts of short-term exposure to O_3. The province-level population and national baseline mortality rate for
244 particular diseases were provided by the National Bureau of Statistics (http://www.stats.gov.cn/). The spatial differences of
245 baseline mortality in China were not considered without provincial-level data, which means that we assume the baseline
246 mortality is evenly distributed across China (Dedoussi et al., 2020). The exposure-response coefficients were obtained from
247 existing epidemiological studies in China (**Table S2**). If the corresponding coefficient of a province could not be found in
248 published epidemiological studies, the datum closest to that province would be selected as a substitute. If there were no
249 neighboring provinces, the results of national meta-analysis would be used (Zhang et al., 2021).

3   Results

3.1 Model development and validation

252   The finally selected features and their importance estimated by the LightGBM algorithm based on 10-fold cross
253 validation are shown in **Fig. 2**. GEOS-Chem-simulated O_3 is the top predictor for predicting surface O_3 concentrations,
254 accounting for 61% and 58% of all relative importance in the ML algorithm predicting hourly O_3 and daily MD8A-O_3,
255 respectively. The result indicates that process-based GEOS-Chem simulations have high utility for O_3 predictions under
256 the hybrid approach (Ma et al., 2021). The meteorological variables with high contribution to both the daily and hourly
257 models are downward surface solar radiation (SSRD), relative humidity at 1000 hpa (RH_1000hpa) and 10-m horizontal
258 wind (U10 and V10). Other special features, including location (latitude and longitude), elevation and diurnal and monthly
259 pattern of O_3, also contribute to ambient O_3 estimations. The spatial distributions of bias-corrected O_3 are consistent with
260 observations for both training and test datasets (**Fig. S2**), indicating that there is no obvious overfitting, i.e., the model is
261 able to generalize from the training set to the test set. The good generalization ability of the model gives us confidence in
262 its ability to make accurate predictions based on new data. In general, the hybrid approach can yield good O_3 estimates in
263 the data-intensive regions, including eastern and central China that are the hotspot areas of O_3 pollution.
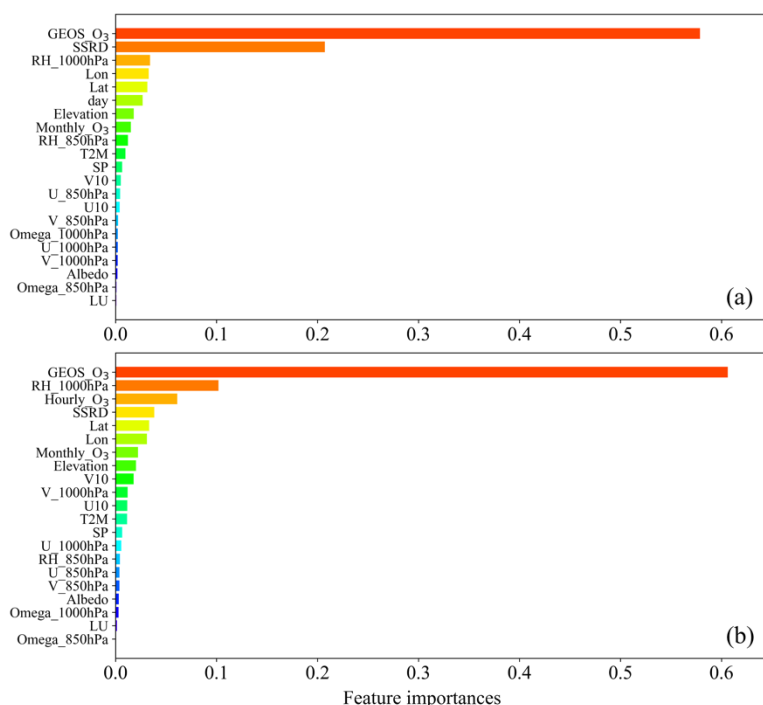
Figure 2. The feature importance plot for (a) MDA8-O₃ and (b) hourly O₃, respectively. The full list of candidate variables with their symbols, units, descriptions, and data sources are shown in Table S3.

Fig. 3 shows the density scatter plots between O₃ measurements and GEOS-Chem simulations, as well as the hybrid-approach predictions for 2018. The R^2 value of the hybrid approach and GEOS-Chem model are 0.66 and 0.27 at hourly level, and 0.72 and 0.53 at MDA8-O₃ level, respectively. Bias-corrected O₃ concentrations have lower RMSE in comparison with GEOS-Chem simulated O₃ concentrations, reduced from 31.1 to 23.8 μg m⁻³ for MDA8-O₃ predictions, and from 38.5 to 26.3 μg m⁻³ for hourly predictions. The MDA8-O₃ model performance is better than that of the hourly model, indicating reduced errors upon temporal averaging. To test if using the higher-resolution meteorological data offers better prediction accuracy compared with the original input meteorology of GEOS-Chem, the MERRA2 dataset driving GEOS-Chem was also used to train the model. We found that the higher-resolution ERA5 dataset performed better in reproducing observed O₃ concentrations with moderately smaller RMSE and larger R^2 (**Fig. S3**), demonstrating the level to which a higher-resolution meteorological dataset, despite not being strictly consistent with the input meteorology for the CTM, can help enhance the performance of the hybrid approach and help resolve finer spatial details within the original CTM grid cells. In summary, the result suggests that the CTM-simulated results can be substantially improved by applying ML with multi-source datasets, and the bias-corrected data can improve our understanding of long-term O₃ trends and its further implications on crop and human health over China, as discussed in the following sections.

In comparison with previous studies, Liu et al. (2020) used XGBoost to predict O₃ in major urban areas of China at a resolution of 0.1°×0.1°, and the R^2 value and RMSE for MDA8-O₃ were 0.74 and 23.8 μg m⁻³, respectively. Their result indicates that higher-resolution predictions may help enhance model accuracy, but represent a trade-off between model accuracy and time efficiency depending on the purpose. Instead of directly predicting O₃ concentrations, Ivatt and Evans (2020) predicted biases in GEOS-Chem-simulated O₃ concentrations and then corrected them with XGBoost. They also suggested that the corrected model performs considerably better than the uncorrected model, with RMSE reduced from 32.4 to 15.0 μg m⁻³ and Pearson's R raised from 0.48 to 0.84. Their greater improvement with larger reduced RMSE than our result is mainly because they selected fewer sites for training, with all the urban and mountain sites (observations made at a pressure < 850 hPa) removed. The removal of these sites can improve the overall apparent performance of the model because O₃ formation could have different characteristics in these areas. In general, ML methods have been proven to be a

291   promising tool to improve air pollutant forecasts when a process-level understanding is still incomplete.
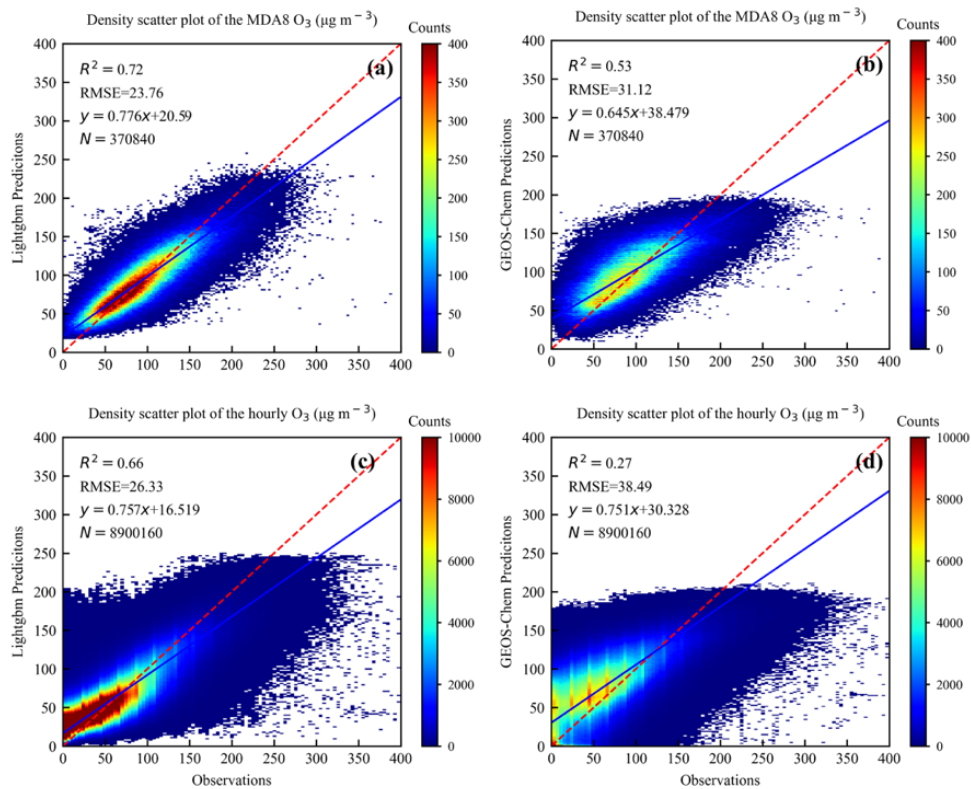
292

293   **Figure 3. Density scatter plots and linear regression statistics of O₃ predictions vs. observation for 2018: (a) bias-**
294   **corrected MDA8-O₃ vs. observations; (b) GEOS-Chem MDA8-O₃ vs. observations; (c) bias-corrected hourly O₃ vs.**
295   **observations; and (d) GEOS-Chem hourly O₃ vs. observations. The model results are sampled at the same locations.**
296   **The dashed red line indicates the 1:1 line, and the solid blue line indicates the line of best fit using orthogonal**
297   **regression. The R^2 is the coefficient of determination, RMSE is the root-mean-square error, and N is the number of**
298   **data points. The X and Y axis represents the O₃ observations and predictions, respectively.**

299

300   **3.2   Spatiotemporal distribution and trends of O₃ predictions**

301   **Fig. 4** demonstrates the spatial patterns of averaged annual and warm-season (May-September) MDA8-O₃ from 1981
302   to 2019. When compared to the high concentrations in the warm season, MDA8-O₃ concentrations are relatively lower at
303   annual level. The annual and warm-season MDA8-O₃ concentrations have similar spatial distribution, and both present an
304   increasing trend over the past decades, with more substantial increase observed between 1981 and 2010. The O₃ levels in
305   southern China are lower than those in northern China, but they are still relatively high in the PRD region, which is
306   consistent to findings in previous studies (e.g. Liu and Wang, 2020a). During the first decade of 1981–1990, high O₃
307   concentration areas are mainly concentrated in the BTHs and northern Shandong. In the next two decades, O₃ pollution
308   extensively expands to most of East and North China, spreading northward to Jilin and Liaoning, westward to Shanxi and
309   Ningxia, and southward to northern Hunan, Shanxi and Zhejiang. Moreover, the SCB and PRD regions also experience
310   aggravated O₃ pollution during this period. In the last decade of the study period, O₃ concentrations remain at high levels
311   in BTHs and SCB without obvious changes. To understand the detailed changes and trends of O₃, next we analyze the
312   interannual variability.

MDA8 O$_3$ (µg m^{-3})
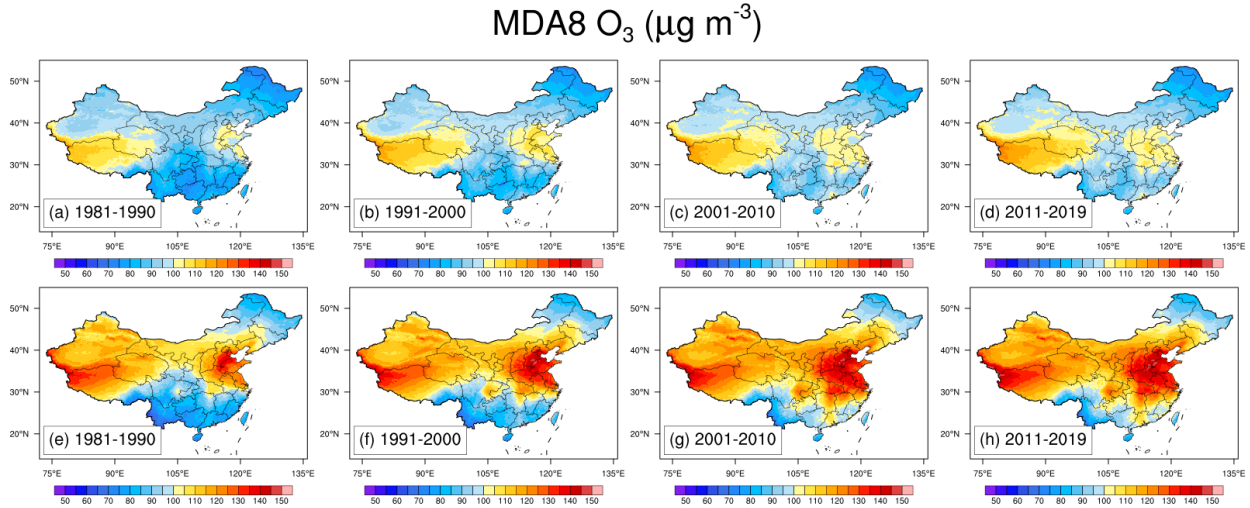
Figure 4. Spatial distribution of the annual mean MDA8-O$_3$ concentrations (µg m^{-3}) during: (a) 1981–1990; (b) 1991–2000; (c) 2001–2010; and (d) 2011–2019. Spatial distribution of the warm-season (May-September) mean MDA8-O$_3$ concentrations of (e)1981–1990, (f) 1991–2000, (g) 2001–2010; and (h) 2011–2019.

Fig. 5 shows that the annual averaged MDA8-O$_3$ concentrations increase from 87 µg m^{-3} in 1981 to 98 µg m^{-3} in 2019, with a growth rate of +0.26 µg m^{-3} yr^{-1}, while the warm-season averaged MDA8-O$_3$ concentrations increase from 100 µg m^{-3} in 1981 to 117 µg m^{-3} in 2019, having a growth rate of +0.51 µg m^{-3} yr^{-1}. Moreover, the average annual and warm-season O$_3$ concentrations have a more obvious upward trend before 2000s, with a growth rate of 0.38 µg m^{-3} yr^{-1} and 0.71 µg m^{-3} yr^{-1}, compared to that after 2000s, when O$_3$ concentrations appear to fluctuate within a certain range. GEOS-Chem-simulated O$_3$ has a similar trend as the bias-corrected O$_3$, but it generally overestimates O$_3$ concentrations on national scale (Fig. S4). The annual and warm-season averaged MDA8-O$_3$ concentrations in BTHs, YRD, SCB and PRD regions are shown in Fig. S5–S6. The warm-season increasing trend for BTHs, YRD, SCB and PRD regions are 0.32 µg m^{-3} yr^{-1}, 0.63 µg m^{-3} yr^{-1}, 0.84 µg m^{-3} yr^{-1}, and 0.81 µg m^{-3} yr^{-1} from the year 1981 to 2019.
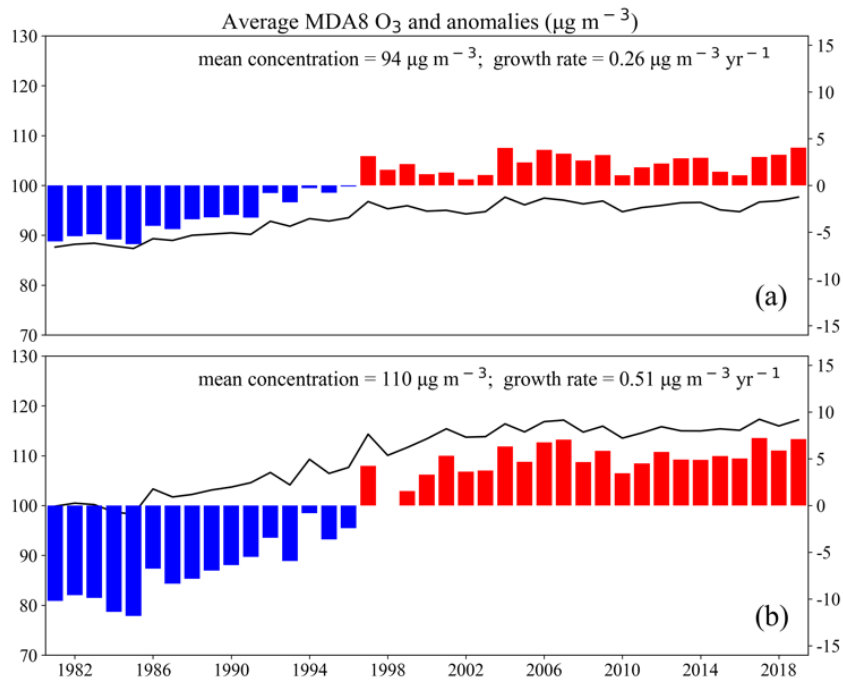
Figure 5. The bias-corrected MDA8-O$_3$ predictions (black line; left y axis) and corresponding anomalies (colored

 bar; right y axis) from 1981 to 2019: (a) annual mean; and (b) warm-season mean (May-September). The trends
329 **(growth rates) are obtained by ordinary linear regression on mean values of MDA8-O$_3$. The anomalies are defined**
330 **as annual mean minus the multidecadal average over 1981–2019.**

331  In recent years, the worsening O$_3$ pollution has fueled numerous studies on ground-level O$_3$ spatial distribution and
332 changes in China, which were conducted on local, regional and national scale using different O$_3$ fields from observations,
333 CTMs and ML estimates. In this study, we mainly focus on the regional and national O$_3$ characteristics, and the reported
334 O$_3$ trends in recent studies are listed in **Table 1**. By comparing the results of existing works, we find that source-varied O$_3$
335 fields can induce great uncertainty of the O$_3$ trends. Moreover, the O$_3$ trends are found to be very sensitive to the study
336 period even with the same O$_3$ fields (Wei et al., 2022), which indicates large interannual variability, mostly reflecting the
337 changing anthropogenic emissions and meteorology (Lu et al., 2019; Li et al., 2020). In contrast to the perceptible O$_3$ trends,
338 Liu et al. (2020) suggested that O$_3$ pollution in most parts of China has only modest changes between 2005 and 2017, and
339 their trends were not spatially continuous. Wang et al. (2022b) also reported that O$_3$ has small positive increase rates for
340 2013–2021 in many cities, and the O$_3$ increase rates greatly differ from site to site even within the same region.

341  In comparison, our results indicate no obvious increasing trends of national MDA8-O$_3$ within the same study period.
342 On a regional scale, only BTHs have a perceptible increasing trend in more recent years, while no such trends are found
343 over the YRD, SCB and PRD regions during the same period. The summertime MDA8-O$_3$ in BTHs has a change rate of
344 +0.81 $\mu g\ m^{-3}\ yr^{-1}$, which is much lower than the results using O$_3$ observations (Li et al., 2020). One possible reason is that
345 most observational sites are in urban regions, which usually suffer more serious O$_3$ pollution, while the O$_3$ concentrations
346 from model simulations and ML methods are calculated on the scale of a grid cell with lower domain-averaged values.
347 Moreover, gridded data at a relatively coarse resolution may fail to capture larger site differences, leading to the larger
348 discrepancy of between O$_3$ observations and gridded O$_3$ estimates.

349 **Table 1 Summary of reported regional and national MDA8-O$_3$ trends ($\mu g\ m^{-3}\ yr^{-1}$).**

Region	Period	Increase rate	Data source/Method	References
Nation	2013–2017 (annual)	0.35	ML (XGBoost)	(Liu et al., 2020)
	2013–2017 (annual)	0.92	WRF-CMAQ	(Liu and Wang, 2020b)
	2013–2017 (annual)	1.33	ML (ERT)	(Wei et al., 2022)
	2015–2019 (annual)	4.40	ML (ERT)	(Wei et al., 2022)
	2015–2019 (annual)	1.90	Observations	(Maji and Namdeo, 2021)
	2013–2019 (summer)	3.80	Observations	(Li et al., 2020)
	1981–2019 (annual)	0.26	ML (LightGBM)	This study
	1981–2000 (annual)	0.38	ML (LightGBM)	This study
	1981–2019 (warm-season)	0.51	ML (LightGBM)	This study
	1981–2000 (warm-season)	0.71	ML (LightGBM)	This study
BTH	2010–2017 (annual)	0.60	ML (Random Forest)	(Ma et al., 2021)
	2013–2017 (annual)	1.33	ML (XGBoost)	(Liu et al., 2020)
	2013–2017 (annual)	4.78	ML (ERT)	(Wei et al., 2022)
	2012–2017 (summer)	1.16	GEOS-Chem	(Dang et al., 2021)
	2013–2019 (summer)	6.60	Observations	(Li et al., 2020)
	1981–2019 (summer)	0.46	ML (LightGBM)	This study
	2013–2019 (summer)	0.81	ML (LightGBM)	This study
YRD	2013–2017 (annual)	2.94	ML (ERT)	(Wei et al., 2022)
	2015–2019 (annual)	5.60	ML (ERT)	(Wei et al., 2022)
	2012–2017 (summer)	3.48	GEOS-Chem	(Dang et al., 2021)
	2013–2019 (summer)	3.20	Observations	(Li et al., 2020)
	1981–2019 (annual)	0.24	ML (LightGBM)	This study
	1981–2019 (summer)	0.73	ML (LightGBM)	This study
SCB	2013–2017 (annual)	2.37	ML (ERT)	(Wei et al., 2022)

	2013–2019 (summer)	1.40	Observations	(Li et al., 2020)
	1981–2019 (annual)	0.48	ML (LightGBM)	This study
	1981–2019 (summer)	0.98	ML (LightGBM)	This study
PRD	2007–2017 (annual)	1.20	Observations	(Yang et al., 2019)
	2013–2017 (annual)	−0.72	ML (ERT)	(Wei et al., 2022)
	2015–2019 (annual)	4.38	ML (ERT)	(Wei et al., 2022)
	2013–2019 (summer)	2.20	Observations	(Li et al., 2020)
	1981–2019 (annual)	0.56	ML (LightGBM)	This study
	1981–2019 (fall)	0.69	ML (LightGBM)	This study

3.3 Seasonal characteristics of O_3 predictions

Differences in averaged annual and warm-season O_3 concentrations indicate that O_3 has distinctive seasonal characteristics. **Fig. 6** shows the seasonal variations in O_3 concentrations from 2011–2019, and results for other past three decades are shown in **Fig. S7-S9**. In winter, pollution is mainly concentrated in the coastal areas of southern China. In spring, O_3 pollution primarily occurs in eastern China and the southern part of Yunnan Province. O_3 pollution continues to aggravate over eastern China in summer, particularly in BTHs, and further extends to SCB. The air quality in eastern and central China is greatly improved in fall, while southern China experiences the most pollution in this period. In general, the peak and trough values of O_3 concentrations appear in summer and winter, respectively. However, O_3 concentrations are found to be minimum in summer and maximum in fall over PRD, which is largely determined by the summer monsoon (Zhou et al., 2013; Wang et al., 2018a). **Fig. S10** shows the seasonal averaged MDA8-O_3 concentrations in different regions from 1981 to 2019. In winter, O_3 concentrations do not have much change across the four regions over the past decades, staying mostly between 70–80 μg m^{-3}. Moreover, wintertime O_3 concentrations after the 2000s are generally lower than that before the 2000s in BTHs, YRD and SCB. In contrast, summertime O_3 concentrations have a dramatic increase over the four regions. In spring and fall, O_3 concentrations have an increasing trend in PRD, while it mostly fluctuates within a certain range in the other three regions. The results show that O_3 in non-winter seasons has a more pronounced increase during 1981–2019 albeit with regional differences. The regional characteristics of O_3 and its influencing factors will be further discussed in Section 3.4. The BTH, SCB, YRD, and PRD regions have been identified as hotspots of O_3 pollution in China. These regions are characterized by high population density (Wang et al., 2018b) and are also major agricultural areas (Monfreda et al., 2008), which may face greater burdens of crop yield and human health losses with high O_3 concentrations. Therefore, here we provide more detailed analysis and investigation of these regions.
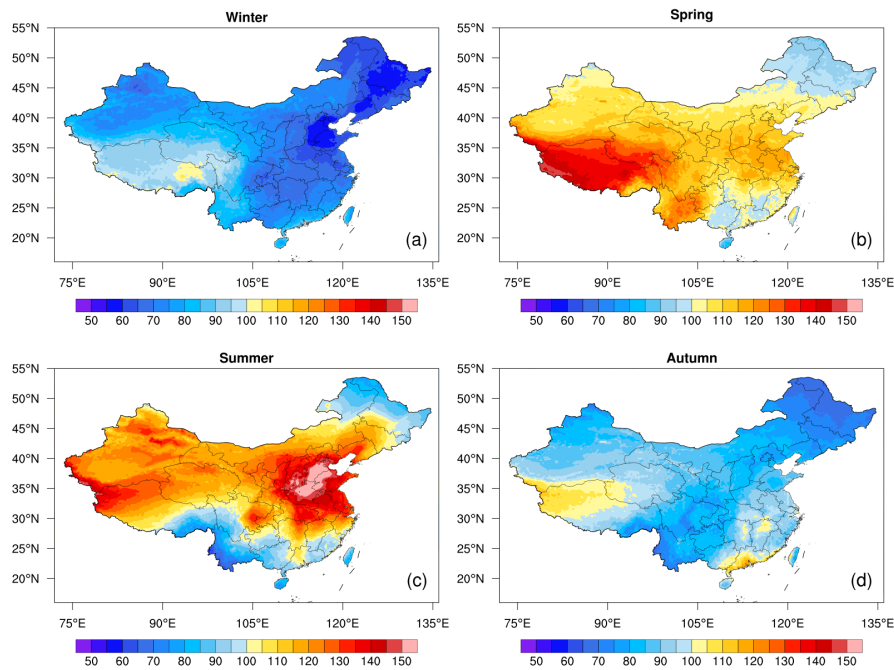
Figure 6. Spatial distribution of the bias-corrected MDA8-O₃ predictions (μg m⁻³) from 2011–2019: (a) winter; (b) spring; (c) summer; and (d) fall.

3.4 Regional characteristics of O₃ predictions

Fig. 7 shows the bar plots of the seasonal MDA8-O₃ concentrations in each region from 1981–2019 for bias-corrected and GEOS-Chem-simulated O₃. For the bias-corrected O₃, the averaged summertime MDA8-O₃ concentrations in BTHs, YRD, SCB and fall-time MDA8-O₃ concentrations in PRD are 137 ± 8 μg m⁻³, 119 ± 10 μg m⁻³, 113 ± 12 μg m⁻³ and 98 ± 10 μg m⁻³, with the increasing rate being 0.46 μg m⁻³ yr⁻¹, 0.73 μg m⁻³ yr⁻¹, 0.98 μg m⁻³ yr⁻¹ and 0.69 μg m⁻³ yr⁻¹ from 1981 to 2019, respectively (**Fig. S11**). For GEOS-Chem-simulated O₃, the averaged summertime MDA8-O₃ concentrations in BTHs, YRD, SCB and fall-time MDA8-O₃ concentrations in PRD are 141 ± 7 μg m⁻³, 125 ± 11 μg m³, 120 ± 14 μg m⁻³ and 100 ± 12 μg m⁻³, respectively. It shows that O₃ concentrations of the four regions have a consistent upward trend in the summer over the past decades, but there are regional differences in other seasons. Compared to BTHs and YRD, PRD and SCB have more distinctive O₃ increases in spring and fall. Among these four regions, the O₃ concentrations in BTHs have the biggest seasonal differences, but have the smallest seasonal differences in PRD.

The spatiotemporal patterns of O₃ in China have been proven to largely depend on both emissions and meteorology. The regional O₃ pollution is usually found to be triggered by specific circulation patterns as local meteorological factors are modulated by synoptic-scale circulation patterns. China has a large territory and is affected by different weather systems. The continental high-pressure systems, components of East Asian summer monsoon (EASM) and tropical cyclones, among others, are critical synoptic conditions leading to O₃ formation and transport in China (Wang et al., 2022b; Han et al., 2020). For instance, regional O₃ pollution in North China usually occurs under a typical weather pattern of an anomalous high-pressure system at 500 hPa (Gong and Liao, 2019), which creates favorable meteorological conditions for high O₃ levels with high temperature, low relative humidity, anomalous southerlies and divergence in the lower troposphere. As one of the most important components of EASM, the Western Pacific subtropical high (WPSH) strongly influences summertime precipitation and atmospheric conditions in East China. A strong WPSH can decrease O₃ levels over YRD as enhanced moisture is transported into YRD under prevailing southwesterly winds (Zhao and Wang, 2017). Located on the southern coast of China, PRD features a typical subtropical monsoon climate. There O₃ concentrations are usually the lowest in summer due to the prevailing southerlies with clean air from the ocean and the associated large rainfall, while the worst O₃

398   pollution usually happens in fall mainly due to the occasional northerly winds during the monsoonal transition, thereby
399   importing precursors from the north, and stable and still relatively warm and sunny weather conditions before the winter
400   starts. Downdrafts in the periphery circulation of a typhoon system can also strongly enhance surface O_3 before typhoon
401   landing (Jiang et al., 2015; Lu et al., 2021; Li et al., 2022). On one the hand, the poor ventilation in the peripheral subsidence
402   region of typhoons favors the accumulation of O_3 and its precursors. On the other hand, the deep subsidence can transport
403   the O_3 in the upper troposphere and lower stratosphere to surface, causing aggravated O_3 pollution. Moreover, smaller-
404   scale circulation patterns, such as land-sea and mountain-valley breezes, also influence O_3 in coastal regions (Ding et al.,
405   2004; Zhou et al., 2013; Wang et al., 2018a).

406   When compared to the hybrid approach, GEOS-Chem generally has similar O_3 distribution and trends over each
407   region, while overestimating O_3 concentrations (**Table S4**). GEOS-Chem particularly overestimates wintertime and fall-
408   time O_3 concentrations in SCB, which are 10 ± 1 µg m^{-3} and 17 ± 3 µg m^{-3} higher than those of the hybrid approach,
409   respectively. Previous studies reported such model overestimates and proposed a number of explanations involving
410   precursor emissions, dry deposition, and vertical mixing in the planetary boundary layer (PBL) (Lin et al., 2008; Travis et
411   al., 2016; Fiore et al., 2005). Both observational analyses and inter-model comparisons suggested that the summertime dry
412   deposition of O_3 calculated by the Wesely scheme in GEOS-Chem could be underestimated, which has been invoked as a
413   cause for model overestimates of O_3. The biased emissions in the model, as consistent with the biased-high tropospheric
414   NO_x columns, result in overestimated O_3. Travis et al. (2016) showed that GEOS-Chem with reduced NO_x emissions
415   provides an unbiased simulation of O_3 observations from the aircraft and reproduces the observed O_3 production efficiency
416   in the boundary layer. Lin et al. (2008) suggested that the excessive PBL mixing can lead to the biased-high O_3
417   concentrations. The fully mixed O_3 throughout the PBL means that the higher O_3 concentrations in the upper PBL are
418   brought down to the surface much more efficiently. Moreover, the excessive spatial averaging of emissions at coarser
419   resolutions could also lead to systematic overestimation of regional O_3 production (Wild and Prather, 2006). In summary,
420   with a higher prediction accuracy, the hybrid approach lends greater credence to using model simulations to extrapolate
421   historical O_3 further back in time, which can furthermore provide us with more accurate estimates of O_3 impacts on crop
422   production and human health.
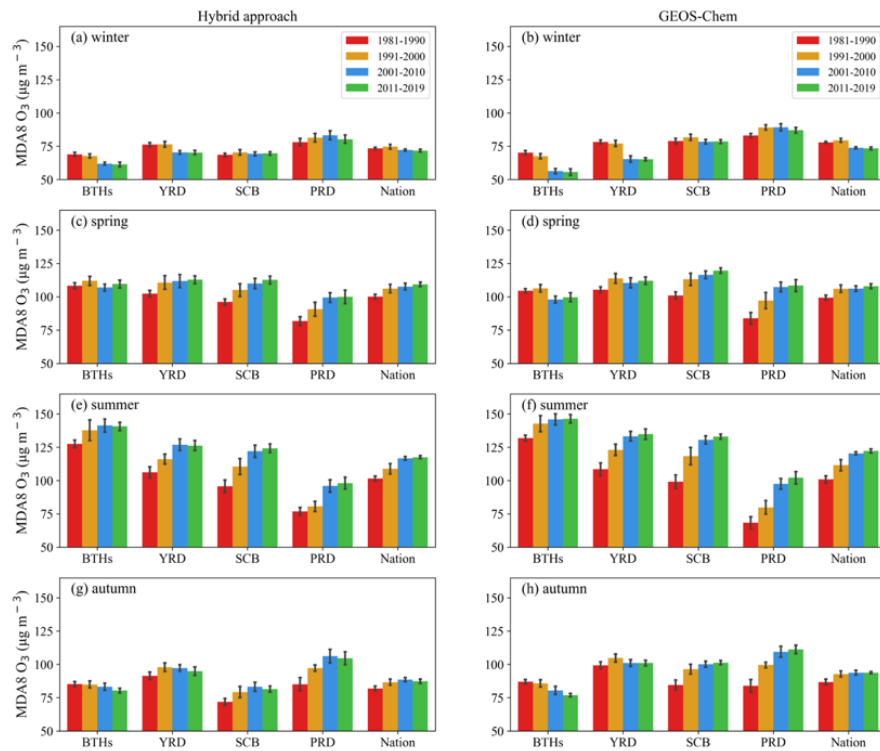
423

3.5 Crop production losses attributable to O₃ pollution

Fig. 8 shows the relative yield losses (RYLs; RYL = 1 – RY, where RY is the relative yield defined as the ratio of the O₃-affected yield to the yield without O₃ exposure) calculated with GEOS-Chem and bias-corrected O₃ using AOT40-China metric. For a given crop, the RYLs show generally consistent spatial distribution across the metrics, with BTHs having the most serious crop yield losses due to high O₃ concentrations. Compared to the bias-corrected O₃, using GEOS-Chem-simulated O₃ generally leads to larger yield losses, especially over BTHs and SCB, reflecting overestimated O₃ concentrations by GEOS-Chem in cropland areas during the growing seasons (**Fig. S12**), primarily in spring and summer, which is consistent to the above analysis. GEOS-Chem-simulated O₃ leads to slightly underestimated wheat yield loss only over some parts of BTHs, mostly because the primary growing period of wheat there is in winter and spring, and GEOS-Chem has lower O₃ estimates than the hybrid approach during this period there (**Table S4**).
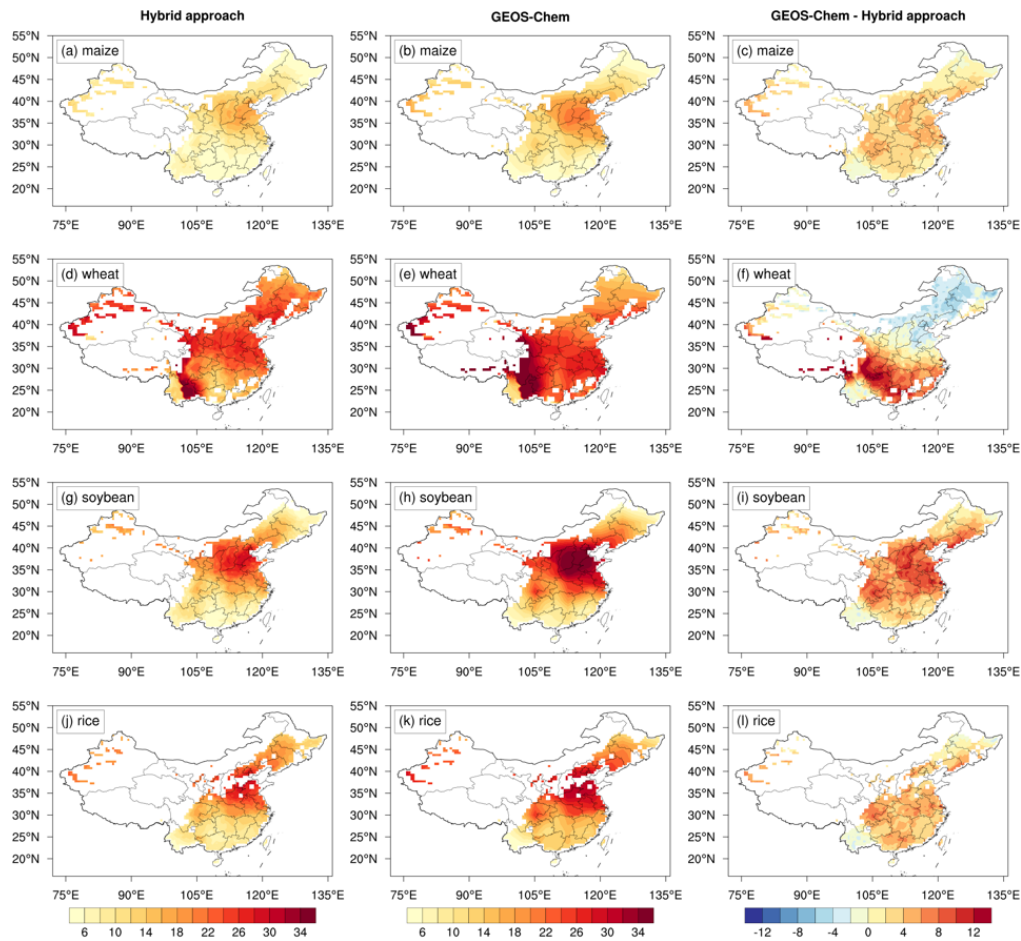
Figure 8. Estimated annual mean relative yield losses (RYLs, in %) of four staple crops from 1981–2019 using the AOT40-China metric. The estimated RYLs using bias-corrected O₃: (a) maize; (d) wheat; (g) soybean; and (j) rice. The estimated RYLs using GEOS-Chem-simulated O₃: (b) maize; (e) wheat; (h) soybean; and (k) rice. The differences in estimated RYLs between GEOS-Chem-simulated and bias-corrected O₃: (c) maize; (f) wheat; (i) soybean; and (l) rice. The GEOS-Chem-simulated O₃ were regridded to 0.5°×0.5° for comparison with bias-corrected O₃.

444   **Fig. 9** shows the bar plots of the relative yield for each crop using AOT40-China exposure-yield response relationship.
445   Crop yield losses are generally consistent with the O_3 trends as the exposure-yield relationships used here are essentially a
446   set of linear functions. Most crops experience aggravated yield losses over the past four decades due to enhanced O_3
447   concentrations, except for wheat, which has the largest yield loss during the period 1991 to 2000. The reason could be that
448   BTHs have the highest O_3 concentrations in spring during the 1990s, which is the primary growing season for wheat (**Fig.
449   S13**). Noticeable uncertainties of crop yield losses are found across metrics.

450   The average annual crop RYLs from 1981 to 2019 for wheat, rice, soybean and maize range from 1.1 to 13.4%, 2.7 to
451   13.4%, 6.3 to 24.8% and 0.8 to 7.4%, respectively. The differences in yield losses across crops reflect the dependence on
452   crop-specific phenology and ecophysiology. The estimated annual RYLs using bias-corrected O_3 for wheat, rice, soybean
453   and maize from 1981 to 2019 range from 17.5–25.5%, 10.7–19.1%, 7.3–17.9% and 7.1–12.7%, with a growth rate of 0.03%
454   yr^{-1}, 0.04% yr^{-1}, 0.27% yr^{-1} and 0.13% yr^{-1}. Wheat is the most sensitive crop to the O_3 concentrations, whereas maize is
455   the least sensitive. Using GEOS-Chem-simulated O_3, the estimated annual RYLs for wheat, rice, soybean and maize from
456   1981 to 2019 are 18.7–28.7%, 14.0–22.0%, 12.4–23.1%, and 7.9–13.2%, having a growth rate of 0.08% yr^{-1}, 0.14% yr^{-1},
457   0.23% yr^{-1} and 0.11% yr^{-1}. There are noticeable differences in crop yield estimates using the bias-corrected and GEOS-
458   Chem O_3, indicating again the importance of the bias-corrected high-resolution O_3 data in related crop issues.

459   In existing studies evaluating the O_3-induced crop losses in China, which also use exposure-yield relationship derived
460   from the experiments conducted in Asia, Zhang et al. (2017) reported that the ambient O_3 concentrations in Northeast China
461   cause substantial annual yield loss of soybean ranging from 23.4% to 30.2% during 2013 and 2014, depending on the O_3
462   metric used (including AOT40, W126, SUM06 and a flux-based metric). Feng et al. (2022), using AOT40, indicated that
463   the annual average RYLs of wheat (33%), rice (23%) and maize (9%) from 2017 to 2019. Our correspondingly estimated
464   RYLs for rice (18.0%) and maize (10.0%) are generally consistent to their results, while the RYLs for soybean (16.4%)
465   and wheat (23.4%) are much lower than the estimates. Since we used the same exposure-yield response relationships in
466   their studies, the discrepancies are primarily attributed to the differences in used metrics (only for soybean), O_3 fields and
467   sensitivity of crop to the changes of O_3 concentrations (Mukherjee et al., 2021; Feng et al., 2022; Mills et al., 2018). In
468   Zhang et al. (2017), the O_3 measurements are obtained from the experimental field (45°73′N, 126°61′E), and in Feng et al.
469   (2022), the measured O_3 concentrations are from over 3,000 monitoring sites across East Asia. The results of comparison
470   are consistent to the previous analysis of O_3 trends and variability from different sources, where the domain-average values
471   of O_3 observations are larger than gridded O_3 from model simulations (**Section 3.2**) and thus lead to larger estimates of
472   RYLs. On one hand, it indicates that O_3 fields should be considered as a great source of uncertainty when comparing the
473   results of previous studies using source-varied O_3 fields. Moreover, different degrees of importance should be given for
474   specific crops, for example, the changes in O_3 concentrations have a larger impact on wheat crop. On the other hand, it
475   highlights again the necessity and importance of bias correction for model-simulated O_3 when O_3-inudec crop reduction.

476
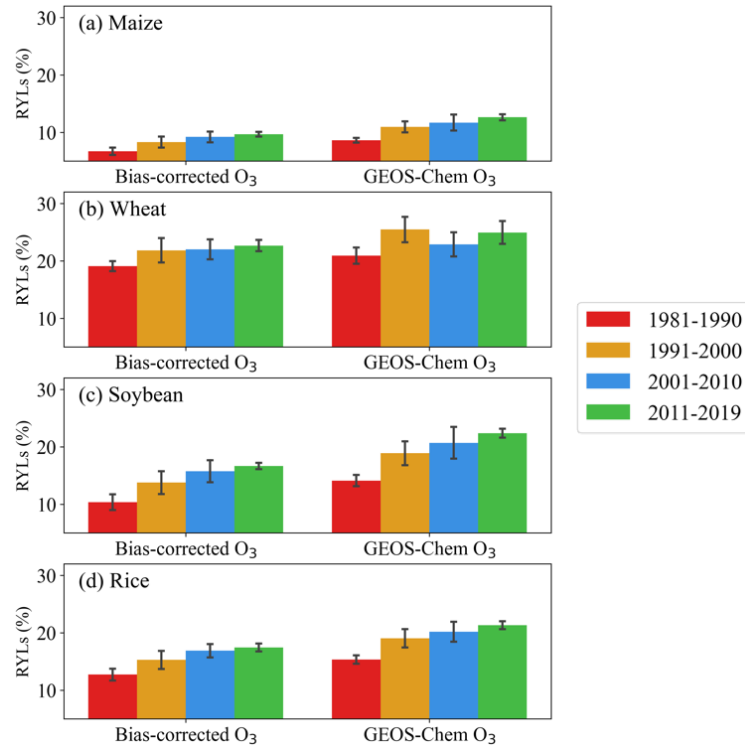
Figure 9. The estimated decadal mean relative yield losses (RYLs) of four staple crops using different metrics from 1981–2019. The estimated RYLs using bias-corrected O₃: (a) maize; (c) wheat; (e) soybean; and (g) rice. The estimated RYLs using GEOS-Chem-simulated O₃: (b) maize; (d) wheat; (f) soybean; and (h) rice. The error bar represents the standard deviation.

3.6 Health impacts attributable to O₃ pollution

The estimated annual all-cause premature deaths induced by O₃ increase from 55,876 in 1981 to 162,370 in 2019 with an increasing trend of +2,979 deaths yr⁻¹. The annual premature deaths related to respiratory and cardiovascular diseases are 34,155 and 40,323 in 1998, and 26,471 and 79,021 in 2019, having a rate of change of –546 and +1,773 deaths yr⁻¹ during 1998–2019, respectively (**Fig. 10a**). Among three types of health outcomes, only respiratory diseases experienced a decreasing trend in premature mortality, and the premature mortality is constantly below 40,000. The decreasing trend of the respiration-related mortality primarily results from the decreased annual baseline mortality rate over the past decades (**Fig. S14**). As the total respiratory-related deaths decreased over the past decades, respiratory O₃ deaths are decreasing even under aggravated O₃ pollution. Based on GEOS-Chem-simulated O₃, the corresponding estimated change rate for all-cause disease is +3,516 deaths yr⁻¹ from 50,384 in 1981 to 176,741 in 2019. Premature mortality induced by respiratory disease decreases from 37,822 in 1998 to 29,079 in 2019 with a change rate of –584 deaths yr⁻¹, while cardiovascular disease increases from 44,516 in 1998 to 85,980 in 2019 with a change rate of +1,977 deaths yr⁻¹ (**Fig. S15**). The result shows that using GEOS-Chem-simulated O₃ generally gives higher estimates of mortality than using the bias-corrected data. **Fig. 10b** shows the provincial annual average premature mortality of different health endpoints. The five provinces with the highest all-cause mortality are Jiangsu [14,510 (95% CI: 9,022–19,935)], Shandong [12,684 (95% CI:4,258–20,990)], Henan [12,290 (95% CI: 4,125–20,343)], Guangdong [9,268 (95% CI: 7,224–11,416)] and Hebei [8,276 (95% CI: 2,776–13,706), which are generally consistent with previous studies for China (Zhang et al., 2021; Zhang et al., 2022a). Similar distribution can be found for respiratory and cardiovascular diseases but with a different ranking order. Generally, those provinces in densely populated areas (**Fig. 10c**) with higher O₃ concentrations, such as BTHs, YRD and PRD, have higher health burdens. In contrast, the northeastern and southern China (excluding Guangdong) suffer the least life losses

501   induced by O_3 exposure (**Fig. S16**).

502   When compared with estimates from previous studies, our estimates of are generally quite consistent with that given

503   by Maji and Namdeo (2021), which reported that the short-term all-cause, cardiovascular and respiratory premature

504   mortalities attributed to ambient O_3 exposure were 156,000, 73,500 and 28,600 in 2019. Based on O_3 observations in 334

505   Chinese cities, Zhang et al. (2021) suggested that the national all-cause, respiratory, cardiovascular mortalities attributable

506   to O_3 are 270,000 to 390,000, 49,000 to 63,000, and 150,000 to 220,000 across 2015–2018, which are much higher than

507   most existing results. Since the methodological approaches are largely similar and we use the log-linear exposure-response

508   function, we ascribe that the very high estimated mortalities are mainly due to concentration–response threshold X_0 assumed

509   to be zero in their study. A lower X_0 means that O_3 can cause more adverse impacts on human health even at low

510   concentrations, thus leading to higher mortalities.

511
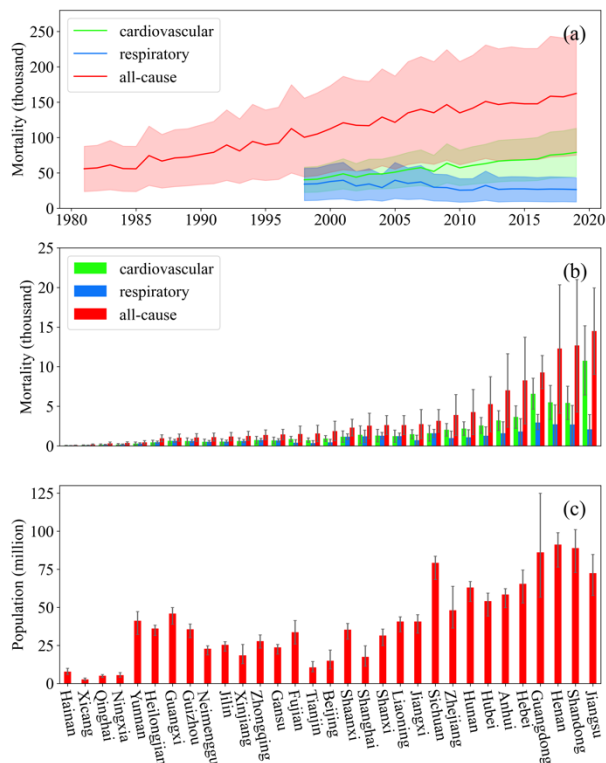
512   **Figure 10. (a) Annual premature morality (thousand) for different diseases over the past decades; (b) annual mean**

513   **province-based morality (thousand) attributed to different health endpoints; and (c) annual mean province-based**

514   **population (million). The morality is calculated using the bias-corrected O_3.**

515   **4.   Conclusions and discussion**

516   In this study, to have a more accurate characterization of O_3 spatiotemporal distribution and trends as well as their

517   impacts on agriculture and human health, we used a hybrid approach to generate bias-corrected O_3 data across China from

518   1981 to 2019. The hybrid approach helps improve O_3 predictions by taking advantage of a chemical transport model, a ML

519   algorithm and increasing availability of high-resolution environmental and meteorological data. In the model training

520   process, we found that utilizing a higher-resolution meteorological dataset, albeit one that is not the same as the default

521   CTM input meteorology, has high potential to enhance the performance of the hybrid model in reproducing observed O_3

522   concentrations. The validation shows that the bias-corrected O_3 can achieve a higher prediction accuracy than GEOS-

523   Chem-simulated O_3 alone when compared with historical in-situ measurements. Before being corrected, the GEOS-Chem-

524   simulated O_3 concentrations tend to be overestimated and lead to higher crop yield losses and larger O_3-induced mortalities.

525 Noticeable differences in crop RYLs and mortality estimates highlight the advantages of using high-resolution O_3 data to
526 improve our understanding of long-term O_3 impacts.

527   When examining the regional and national O_3 trends, we found that MDA8-O_3 concentrations have a perceptible
528 increasing trend before 2000s, but fluctuate within a certain range with large interannual variabilities in more recent years.
529 The large discrepancies in previous studies indicate that the regional and national O_3 trends in China still suffer with great
530 uncertainties, particularly when different approaches are used to produce the O_3 estimates. However, these studies using
531 source-varied O_3 fields consistently show the great interannual variabilities of O_3 concentrations. Some insights can be
532 obtained from existing findings, which need to be carefully considered when examining O_3 trends and comparing them
533 with existing results. First, given the large site differences, the calculation of observational O_3 trends is very sensitive to
534 the subsets of data from networks. Thus, great uncertainty could still exist even using O_3 observations from the same source
535 depending on the chosen subsets of data. Second, different formats of O_3 fields (e.g., site-based and gridded) could lead to
536 large uncertainties of the O_3 trend estimates. A higher resolution of gridded O_3 estimates from CTMs and ML may reduce
537 the differences between O_3 observational results. Third, the calculated O_3 trends are very sensitive to the chosen study
538 period due to large interannual variability and seasonal differences. The changing meteorological conditions are the major
539 factor causing the large interannual O_3 variations, and reductions in the emissions of NO_x, SO_2 and PM also have complex
540 effects on ground-level O_3 concentrations (Wang et al., 2022b). Liu and Wang (2020a) suggested that the meteorological
541 impacts on O_3 trends vary region by region and year by year and could be comparable with or even larger than the impacts
542 of changes in anthropogenic emissions.

543   Our estimated RYLs for maize and rice and soybean in China are generally consistent to existing studies, while the
544 RYLs for soybean and wheat are lower than their estimates mainly due to the differences in used metrics, O_3 fields and
545 crop sensitivity to ambient O_3 concentrations. It suggests that plating O_3-resistant cultivars could be an effective approach
546 to increase total crop production to meet the increasing food demands. In addition to the metrics and O_3 fields, uncertainties
547 of estimated O_3-induced crop losses could be also from other sources (e.g., exposure-yield relationships). Though some
548 other metrics (e.g., M7/M12 and W126) have also been used in some studies (Van Dingenen et al., 2009; Avnery et al.,
549 2013; Wang et al., 2022c), there are not available exposure-yield relationships for all four major crops specific for China.
550 The estimated RYLs for crops could be largely biased using metrics with exposure-yield relationships developed for U.S.
551 or Europe (**Fig. S17**), as they are inadequate to represent Asian crop genotypes and environmental conditions. So, the
552 region-specific exposure-yield relationships are highly recommended to be used in future study estimating the O_3-induced
553 crop reduction, especially for the regional study.

554   In recent years, although existing studies have made efforts to quantify the O_3-related health impacts in China, only a
555 few focused on the nationwide acute O_3 health burden assessment, particularly for assessment over multiple decades (Maji
556 and Namdeo, 2021; Sahu et al., 2021; Zhang et al., 2021; Zhang et al., 2022a). There are some remaining issues to be
557 addressed regarding O_3 health impacts. For instance, the existence of a "safe" threshold of O_3 levels still remains debated.
558 A recent study reported that no consistent evidence was found for a threshold in the O_3-mortality concentration-response
559 relationship in seven cities of Jiangsu Province, China during 2013–2014 (Chen et al., 2017; Maji and Namdeo, 2021).
560 Given the importance of the threshold assumption in assessing health effects of air pollution, more studies are needed to
561 determine a most likely threshold for O_3-mortality association in the future. Moreover, the multiple temporal O_3 metrics
562 (e.g.,1-h maximum and daytime average O_3 concentrations) have also been proved to play an important role in the
563 variability of estimated health effects, even though standard ratios are used to convert among multiple metrics (Anderson
564 and Bell, 2010). In addition to the uncertainties from varying methodologies, interpretation of the O_3 epidemiological
565 impact is also constrained by the variability in geographical, seasonal, and demographic characteristics (Yin et al., 2017b).
566 Liu et al. (2013) suggested that associations between O_3 and mortality appeared to be more evident during the cool season
567 than in the warm season, and stronger in the oldest age group and among those with less education. The effect modification

568 by population susceptibility and the confounding effects of concomitant exposures (temperature, particulate matter, etc.)
569 should be further considered in future works.

570 A major limitation of our study lies in the uncertain predictions in regions where monitoring data are scarce (e.g., the
571 western half of China). The monitoring sites are sparsely distributed in those areas, which may fail to capture the accurate
572 association between O_3 concentrations and various predictors there, especially considering that the ML algorithm has likely
573 over-emphasized such relationships in the data-intensive eastern regions. Second, the land use data were prescribed in 2013
574 due to the limited availability of data, and this may neglect some major land use changes in China over the past decades.
575 Though the land use data were found by the ML algorithm to contribute little to the overall model, more detailed land use
576 data are expected to further increase model accuracy. In addition, though concentration-based metrics are easy to calculate
577 and ensured to be scientifically sound in some experiments (Fuhrer et al., 1997; Mills et al., 2007), they do not consider
578 the active responses of plant ecophysiology to ambient climatic and environmental changes and thus likely inadequate for
579 examining yield losses in a future climate and atmospheric environment (Tai et al., 2021). So, flux-based metrics are
580 recommended in future studies to better understand the long-term evolution of crop losses over China (Feng et al., 2012;
581 Zhang et al., 2017; Tai et al., 2021; Pleijel et al., 2022), wherein more crop- and region-specific experiments and trials are
582 needed to acquire appropriate metrics and exposure-yield response functions and calibrate the process-based crop model.

583 Despite these limitations, our study represents important progress in evaluating the long-term, multidecadal health
584 burdens and agricultural losses resulting from O_3 pollution in China. Across the four major regions, BTHs experience the
585 highest RYLs for major crops due to elevated O_3. On the other hand, the YRD and PRD regions have greater human health
586 losses primarily due to their large population size. The results can provide important references for governments and
587 agencies when making related national or regional policies to meet the imperative environment, health, and food security
588 demands. To effectively address O_3 impacts, collaborative efforts can be made in multifaceted aspects: (1) to implement
589 stricter regulations and specific emission control measures for major ozone precursors from industrial, vehicular and
590 agricultural sources that account for region-specific chemical, meteorological and terrestrial conditions; (2) to encourage
591 the adoption of more sustainable and adaptive agricultural practices that minimize O_3 exposure and its damage on crops
592 (e.g., cultivating O_3-resistant crop varieties); (3) to improve short-range O_3 forecast capabilities of regional models,
593 especially with the enhancement of artificial intelligence technology, which may enable better early warning systems to
594 prepare the public and farmers for O_3 episodes; (4) to raise public awareness via promotional campaigns and educational
595 programs to inform individuals, communities, and farmers about the risks associated with O_3. It is important for
596 policymakers to consider these suggestions and act to effectively mitigate the negative O_3 impacts.

597 **Data availability.** Model output data used for analysis and plotting are available on the open-access online repository:
598 ml_simulated_ozone_China.

599 **Competing interests.** The authors declare that neither they nor their co-authors have any competing interests. At least one
600 of the (co-)authors is a member of the editorial board of Atmospheric Chemistry and Physics.

601 **Author contributions.** APKT designed the study and supervised the writing of the paper. JM conducted model simulation,
602 analyzed results, and wrote the draft with the assistance of TGY and KTC. DHYY performed the GEOS-Chem simulations.
603 ZZF assisted in the interpretation of the results. All authors contributed to the discussion and improvement of the paper.

604 **Acknowledgements**. This work was supported by the National Natural Science Foundation of China (NSFC)/Research
605 Grants Council (RGC) Joint Research Scheme (reference #: N_CUHK440/20, 42061160479) awarded to A. P. K. Tai and
606 Z. Feng.

References

Abdullah, S., Ismail, M., and Fong, S. Y.: Multiple Linear Regression (MLR) models for long term PM10 concentration forecasting during different monsoon seasons, Journal of Sustainability Science and Management, 12, 60-69, 2017.

Accadia, C., Mariani, S., Casaioli, M., Lavagnini, A., and Speranza, A.: Sensitivity of Precipitation Forecast Skill Scores to Bilinear Interpolation and a Simple Nearest-Neighbor Average Method on High-Resolution Verification Grids, Weather and Forecasting, 18, 918-932, https://doi.org/10.1175/1520-0434(2003)018<0918:SOPFSS>2.0.CO;2, 2003.

Anderson, G. B. and Bell, M. L.: Does one size fit all? The suitability of standard ozone exposure metric conversion ratios and implications for epidemiology, Journal of Exposure Science & Environmental Epidemiology, 20, 2-11, https://doi.org/10.1038/jes.2008.69, 2010.

Avnery, S., Mauzerall, D. L., and Fiore, A. M.: Increasing global agricultural production by reducing ozone damages via methane emission controls and ozone-resistant cultivar selection, Global Change Biology, 19, 1285-1299, https://doi.org/10.1111/gcb.12118, 2013.

Bey, I., Jacob, D. J., Yantosca, R. M., Logan, J. A., Field, B. D., Fiore, A. M., Li, Q., Liu, H. Y., Mickley, L. J., and Schultz, M. G.: Global modeling of tropospheric chemistry with assimilated meteorology: Model description and evaluation, Journal of Geophysical Research: Atmospheres, 106, 23073-23095, https://doi.org/10.1029/2001JD000807, 2001.

Bi, J., Knowland, K. E., Keller, C. A., and Liu, Y.: Combining Machine Learning and Numerical Simulation for High-Resolution PM2.5 Concentration Forecast, Environ Sci Technol, 56, 1544-1556, https://doi.org/10.1021/acs.est.1c05578, 2022.

Chen, K., Zhou, L., Chen, X., Bi, J., and Kinney, P. L.: Acute effect of ozone exposure on daily mortality in seven cities of Jiangsu Province, China: No clear evidence for threshold, Environmental Research, 155, 235-241, https://doi.org/10.1016/j.envres.2017.02.009, 2017.

Chen, T. and Guestrin, C.: XGBoost: A Scalable Tree Boosting System, Proceedings of the 22nd ACM SIGKDD International Conference on Knowledge Discovery and Data Mining, San Francisco, California, USA, https://doi.org/10.1145/2939672.2939785, 2016.

Clifton, O. E., Fiore, A. M., Massman, W. J., Baublitz, C. B., Coyle, M., Emberson, L., Fares, S., Farmer, D. K., Gentine, P., Gerosa, G., Guenther, A. B., Helmig, D., Lombardozzi, D. L., Munger, J. W., Patton, E. G., Pusede, S. E., Schwede, D. B., Silva, S. J., Sorgel, M., Steiner, A. L., and Tai, A. P. K.: Dry Deposition of Ozone over Land: Processes, Measurement, and Modeling, Rev Geophys, 58, https://doi.org/10.1029/2019RG000670, 2020.

Dang, R., Liao, H., and Fu, Y.: Quantifying the anthropogenic and meteorological influences on summertime surface ozone in China over 2012–2017, Science of The Total Environment, 754, 142394, https://doi.org/10.1016/j.scitotenv.2020.142394, 2021.

Dedoussi, I. C., Eastham, S. D., Monier, E., and Barrett, S. R. H.: Premature mortality related to United States cross-state air pollution, Nature, 578, 261-265, https://doi.org/10.1038/s41586-020-1983-8, 2020.

Di, Q., Rowland, S., Koutrakis, P., and Schwartz, J.: A hybrid model for spatially and temporally resolved ozone exposures in the continental United States, Journal of the Air & Waste Management Association, 67, 39-52, https://doi.org/10.1080/10962247.2016.1200159, 2017.

Ding, A., Wang, T., Zhao, M., Wang, T., and Li, Z.: Simulation of sea-land breezes and a discussion of their implications on the transport of air pollution during a multi-day ozone episode in the Pearl River Delta of China, Atmospheric Environment, 38, 6737-6750, https://doi.org/10.1016/j.atmosenv.2004.09.017, 2004.

Emberson, L. D., Büker, P., Ashmore, M. R., Mills, G., Jackson, L. S., Agrawal, M., Atikuzzaman, M. D., Cinderby, S., Engardt, M., Jamir, C., Kobayashi, K., Oanh, N. T. K., Quadir, Q. F., and Wahid, A.: A comparison of North American and Asian exposure–response data for ozone effects on crop yields, Atmospheric Environment, 43, 1945-1953, https://doi.org/10.1016/j.atmosenv.2009.01.005, 2009.

Feng, Z., Calatayud, V., Zhu, J., and Kobayashi, K.: Ozone exposure- and flux-based response relationships with

651   photosynthesis of winter wheat under fully open air condition, Science of The Total Environment, 619-620, 1538-
652   1544, https://doi.org/10.1016/j.scitotenv.2017.10.089, 2018.

653 Feng, Z., Tang, H., Uddling, J., Pleijel, H., Kobayashi, K., Zhu, J., Oue, H., and Guo, W.: A stomatal ozone flux–response
654   relationship to assess ozone-induced yield loss of winter wheat in subtropical China, Environmental Pollution, 164,
655   16-23, https://doi.org/10.1016/j.envpol.2012.01.014, 2012.

656 Feng, Z., De Marco, A., Anav, A., Gualtieri, M., Sicard, P., Tian, H., Fornasier, F., Tao, F., Guo, A., and Paoletti, E.:
657   Economic losses due to ozone impacts on human health, forest productivity and crop yield across China, Environ Int,
658   131, 104966, https://doi.org/10.1016/j.envint.2019.104966, 2019.

659 Feng, Z., Xu, Y., Kobayashi, K., Dai, L., Zhang, T., Agathokleous, E., Calatayud, V., Paoletti, E., Mukherjee, A., Agrawal,
660   M., Park, R. J., Oak, Y. J., and Yue, X.: Ozone pollution threatens the production of major staple crops in East Asia,
661   Nature Food, 3, 47-56, https://doi.org/10.1038/s43016-021-00422-6, 2022.

662 Fiore, A. M., Horowitz, L. W., Purves, D. W., Levy Ii, H., Evans, M. J., Wang, Y., Li, Q., and Yantosca, R. M.: Evaluating
663   the contribution of changes in isoprene emissions to surface ozone trends over the eastern United States, Journal of
664   Geophysical Research: Atmospheres, 110, https://doi.org/10.1029/2004JD005485, 2005.

665 Fu, Y. and Tai, A. P. K.: Impact of climate and land cover changes on tropospheric ozone air quality and public health in
666   East Asia between 1980 and 2010, Atmos. Chem. Phys., 15, 10093-10106, https://doi.org/10.5194/acp-15-10093-2015,
667   2015.

668 Fuhrer, J., Skärby, L., and Ashmore, M. R.: Critical levels for ozone effects on vegetation in Europe, Environmental
669   Pollution, 97, 91-106, https://doi.org/10.1016/S0269-7491(97)00067-5, 1997.

670 Fusco, A. C. and Logan, J. A.: Analysis of 1970–1995 trends in tropospheric ozone at Northern Hemisphere midlatitudes
671   with the GEOS-CHEM model, Journal of Geophysical Research: Atmospheres, 108,
672   https://doi.org/10.1029/2002JD002742, 2003.

673 Gong, C. and Liao, H.: A typical weather pattern for ozone pollution events in North China, Atmos. Chem. Phys., 19,
674   13725-13740, https://doi.org/10.5194/acp-19-13725-2019, 2019.

675 Gong, C., Yue, X., Liao, H., and Ma, Y.: A humidity-based exposure index representing ozone damage effects on vegetation,
676   Environmental Research Letters, 16, https://doi.org/10.1088/1748-9326/abecbb, 2021.

677 Guenther, A. B., Jiang, X., Heald, C. L., Sakulyanontvittaya, T., Duhl, T., Emmons, L. K., and Wang, X.: The Model of
678   Emissions of Gases and Aerosols from Nature version 2.1 (MEGAN2.1): an extended and updated framework for
679   modeling biogenic emissions, Geosci. Model Dev., 5, 1471-1492, https://doi.org/10.5194/gmd-5-1471-2012, 2012.

680 Han, H., Liu, J., Shu, L., Wang, T., and Yuan, H.: Local and synoptic meteorological influences on daily variability in
681   summertime surface ozone in eastern China, Atmos. Chem. Phys., 20, 203-222, https://doi.org/10.5194/acp-20-203-
682   2020, 2020.

683 He, J., Wang, Y., Hao, J., Shen, L., and Wang, L.: Variations of surface O_3 in August at a rural site near Shanghai: influences
684   from the West Pacific subtropical high and anthropogenic emissions, Environmental Science and Pollution Research,
685   19, 4016-4029, https://doi.org/10.1007/s11356-012-0970-5, 2012.

686 Hoesly, R. M., Smith, S. J., Feng, L., Klimont, Z., Janssens-Maenhout, G., Pitkanen, T., Seibert, J. J., Vu, L., Andres, R. J.,
687   Bolt, R. M., Bond, T. C., Dawidowski, L., Kholod, N., Kurokawa, J. I., Li, M., Liu, L., Lu, Z., Moura, M. C. P.,
688   O'Rourke, P. R., and Zhang, Q.: Historical (1750–2014) anthropogenic emissions of reactive gases and aerosols from
689   the Community Emissions Data System (CEDS), Geosci. Model Dev., 11, 369-408, https://doi.org/10.5194/gmd-11-
690   369-2018, 2018.

691 Hu, X., Belle, J. H., Meng, X., Wildani, A., Waller, L. A., Strickland, M. J., and Liu, Y.: Estimating PM2.5 Concentrations
692   in the Conterminous United States Using the Random Forest Approach, Environ Sci Technol, 51, 6936-6944,
693   https://doi.org/10.1021/acs.est.7b01210, 2017.

694 Irrgang, C., Boers, N., Sonnewald, M., Barnes, E. A., Kadow, C., Staneva, J., and Saynisch-Wagner, J.: Towards neural

Earth system modelling by integrating artificial intelligence in Earth system science, Nature Machine Intelligence, 3, 667-674, https://doi.org/10.1038/s42256-021-00374-3, 2021.

Ivatt, P. D. and Evans, M. J.: Improving the prediction of an atmospheric chemistry transport model using gradient-boosted regression trees, Atmos. Chem. Phys., 20, 8063-8082, https://doi.org/10.5194/acp-20-8063-2020, 2020.

Jacob, D. J. and Winner, D. A.: Effect of climate change on air quality, Atmospheric Environment, 43, 51-63, https://doi.org/10.1016/j.atmosenv.2008.09.051, 2009.

Jiang, Y. C., Zhao, T. L., Liu, J., Xu, X. D., Tan, C. H., Cheng, X. H., Bi, X. Y., Gan, J. B., You, J. F., and Zhao, S. Z.: Why does surface ozone peak before a typhoon landing in southeast China?, Atmos. Chem. Phys., 15, 13331-13338, https://doi.org/10.5194/acp-15-13331-2015, 2015.

Kawase, H., Nagashima, T., Sudo, K., and Nozawa, T.: Future changes in tropospheric ozone under Representative Concentration Pathways (RCPs), Geophysical Research Letters, 38, https://doi.org/10.1029/2010GL046402, 2011.

Lelieveld, J., Evans, J. S., Fnais, M., Giannadaki, D., and Pozzer, A.: The contribution of outdoor air pollution sources to premature mortality on a global scale, Nature, 525, 367-371, https://doi.org/10.1038/nature15371, 2015.

Li, K., Jacob, D. J., Shen, L., Lu, X., De Smedt, I., and Liao, H.: Increases in surface ozone pollution in China from 2013 to 2019: anthropogenic and meteorological influences, Atmos. Chem. Phys., 20, 11423-11433, https://doi.org/10.5194/acp-20-11423-2020, 2020.

Li, K., Jacob, D. J., Liao, H., Qiu, Y., Shen, L., Zhai, S., Bates, K. H., Sulprizio, M. P., Song, S., Lu, X., Zhang, Q., Zheng, B., Zhang, Y., Zhang, J., Lee, H. C., and Kuk, S. K.: Ozone pollution in the North China Plain spreading into the late-winter haze season, Proceedings of the National Academy of Sciences, 118, e2015797118, 10.1073/pnas.2015797118, 2021.

Li, Y., Zhao, X., Deng, X., and Gao, J.: The impact of peripheral circulation characteristics of typhoon on sustained ozone episodes over the Pearl River Delta region, China, Atmos. Chem. Phys., 22, 3861-3873, https://doi.org/10.5194/acp-22-3861-2022, 2022.

Lin, J. T., Youn, D., Liang, X. Z., and Wuebbles, D. J.: Global model simulation of summertime U.S. ozone diurnal cycle and its sensitivity to PBL mixing, spatial resolution, and emissions, Atmospheric Environment, 42, 8470-8483, https://doi.org/10.1016/j.atmosenv.2008.08.012, 2008.

Liu, H., Liu, S., Xue, B., Lv, Z., Meng, Z., Yang, X., Xue, T., Yu, Q., and He, K.: Ground-level ozone pollution and its health impacts in China, Atmospheric Environment, 173, 223-230, https://doi.org/10.1016/j.atmosenv.2017.11.014, 2018.

Liu, J., Wang, L., Li, M., Liao, Z., Sun, Y., Song, T., Gao, W., Wang, Y., Li, Y., Ji, D., Hu, B., Kerminen, V. M., Wang, Y., and Kulmala, M.: Quantifying the impact of synoptic circulation patterns on ozone variability in northern China from April to October 2013–2017, Atmos. Chem. Phys., 19, 14477-14492, https://doi.org/10.5194/acp-19-14477-2019, 2019.

Liu, R., Ma, Z., Liu, Y., Shao, Y., Zhao, W., and Bi, J.: Spatiotemporal distributions of surface ozone levels in China from 2005 to 2017: A machine learning approach, Environ Int, 142, 105823, https://doi.org/10.1016/j.envint.2020.105823, 2020.

Liu, T., Li, T. T., Zhang, Y. H., Xu, Y. J., Lao, X. Q., Rutherford, S., Chu, C., Luo, Y., Zhu, Q., Xu, X. J., Xie, H. Y., Liu, Z. R., and Ma, W. J.: The short-term effect of ambient ozone on mortality is modified by temperature in Guangzhou, China, Atmospheric Environment, 76, 59-67, https://doi.org/10.1016/j.atmosenv.2012.07.011, 2013.

Liu, Y. and Wang, T.: Worsening urban ozone pollution in China from 2013 to 2017 – Part 1: The complex and varying roles of meteorology, Atmos. Chem. Phys., 20, 6305-6321, https://doi.org/10.5194/acp-20-6305-2020, 2020a.

Liu, Y. and Wang, T.: Worsening urban ozone pollution in China from 2013 to 2017 – Part 2: The effects of emission changes and implications for multi-pollutant control, Atmos. Chem. Phys., 20, 6323-6337, https://doi.org/10.5194/acp-20-6323-2020, 2020b.

739 Lu, C., Mao, J., Wang, L., Guan, Z., Zhao, G., and Li, M.: An unusual high ozone event over the North and Northeast China
740 during the record-breaking summer in 2018, J Environ Sci (China), 104, 264-276,
741 https://doi.org/10.1016/j.jes.2020.11.030, 2021.

742 Lu, X., Hong, J., Zhang, L., Cooper, O. R., Schultz, M. G., Xu, X., Wang, T., Gao, M., Zhao, Y., and Zhang, Y.: Severe
743 Surface Ozone Pollution in China: A Global Perspective, Environmental Science & Technology Letters, 5, 487-494,
744 https://doi.org/10.1021/acs.estlett.8b00366, 2018.

745 Lu, X., Zhang, L., Chen, Y., Zhou, M., Zheng, B., Li, K., Liu, Y., Lin, J., Fu, T.-M., and Zhang, Q.: Exploring 2016–2017
746 surface ozone pollution over China: source contributions and meteorological influences, Atmos. Chem. Phys., 19,
747 8339-8361, https://doi.org/10.5194/acp-19-8339-2019, 2019.

748 Ma, R., Ban, J., Wang, Q., Zhang, Y., Yang, Y., He, M. Z., Li, S., Shi, W., and Li, T.: Random forest model based fine scale
749 spatiotemporal O_3 trends in the Beijing-Tianjin-Hebei region in China, 2010 to 2017, Environmental Pollution, 276,
750 116635, https://doi.org/10.1016/j.envpol.2021.116635, 2021.

751 Madaniyazi, L., Nagashima, T., Guo, Y., Pan, X., and Tong, S.: Projecting ozone-related mortality in East China,
752 Environment International, 92-93, 165-172, https://doi.org/10.1016/j.envint.2016.03.040, 2016.

753 Maji, K. J. and Namdeo, A.: Continuous increases of surface ozone and associated premature mortality growth in China
754 during 2015–2019, Environmental Pollution, 269, 116183, https://doi.org/10.1016/j.envpol.2020.116183, 2021.

755 Mao, J., Wang, L., Lu, C., Liu, J., Li, M., Tang, G., Ji, D., Zhang, N., and Wang, Y.: Meteorological mechanism for a large-
756 scale persistent severe ozone pollution event over eastern China in 2017, J Environ Sci (China), 92, 187-199,
757 https://doi.org/10.1016/j.jes.2020.02.019, 2020.

758 Mills, G., Buse, A., Gimeno, B., Bermejo, V., Holland, M., Emberson, L., and Pleijel, H.: A synthesis of AOT40-based
759 response functions and critical levels of ozone for agricultural and horticultural crops, Atmospheric Environment, 41,
760 2630-2643, https://doi.org/10.1016/j.atmosenv.2006.11.016, 2007.

761 Mills, G., Sharps, K., Simpson, D., Pleijel, H., Frei, M., Burkey, K., Emberson, L., Uddling, J., Broberg, M., Feng, Z.,
762 Kobayashi, K., and Agrawal, M.: Closing the global ozone yield gap: Quantification and cobenefits for multistress
763 tolerance, Global Change Biology, 24, 4869-4893, https://doi.org/10.1111/gcb.14381, 2018.

764 Monfreda, C., Ramankutty, N., and Foley, J. A.: Farming the planet: 2. Geographic distribution of crop areas, yields,
765 physiological types, and net primary production in the year 2000, Global Biogeochemical Cycles, 22,
766 https://doi.org/10.1029/2007GB002947, 2008.

767 Moustris, K. P., Nastos, P. T., Larissi, I. K., and Paliatsos, A. G.: Application of Multiple Linear Regression Models and
768 Artificial Neural Networks on the Surface Ozone Forecast in the Greater Athens Area, Greece, Advances in
769 Meteorology, 2012, 894714, https://doi.org/10.1155/2012/894714, 2012.

770 Mukherjee, A., Yadav, D. S., Agrawal, S. B., and Agrawal, M.: Ozone a persistent challenge to food security in India:
771 Current status and policy implications, Current Opinion in Environmental Science & Health, 19, 100220,
772 https://doi.org/10.1016/j.coesh.2020.10.008, 2021.

773 Pleijel, H., Danielsson, H., and Broberg, M. C.: Benefits of the Phytotoxic Ozone Dose (POD) index in dose-response
774 functions for wheat yield loss, Atmospheric Environment, 268, 118797,
775 https://doi.org/10.1016/j.atmosenv.2021.118797, 2022.

776 Sacks, W. J., Deryng, D., Foley, J. A., and Ramankutty, N.: Crop planting dates: an analysis of global patterns, Global
777 Ecology and Biogeography, 19, 607-620, https://doi.org/10.1111/j.1466-8238.2010.00551.x, 2010.

778 Sahu, S. K., Liu, S., Liu, S., Ding, D., and Xing, J.: Ozone pollution in China: Background and transboundary contributions
779 to ozone concentration & related health effects across the country, Sci Total Environ, 761, 144131,
780 https://doi.org/10.1016/j.scitotenv.2020.144131, 2021.

781 Shang, Y., Sun, Z., Cao, J., Wang, X., Zhong, L., Bi, X., Li, H., Liu, W., Zhu, T., and Huang, W.: Systematic review of
782 Chinese studies of short-term exposure to air pollution and daily mortality, Environment International, 54, 100-111,

783   https://doi.org/10.1016/j.envint.2013.01.010, 2013.

784 Sindelarova, K., Granier, C., Bouarar, I., Guenther, A., Tilmes, S., Stavrakou, T., Müller, J. F., Kuhn, U., Stefani, P., and

785   Knorr, W.: Global data set of biogenic VOC emissions calculated by the MEGAN model over the last 30 years, Atmos.

786   Chem. Phys., 14, 9317-9341, https://doi.org/10.5194/acp-14-9317-2014, 2014.

787 Tai, A. P. K., Mickley, L. J., Heald, C. L., and Wu, S.: Effect of CO_2 inhibition on biogenic isoprene emission: Implications

788   for air quality under 2000 to 2050 changes in climate, vegetation, and land use, Geophysical Research Letters, 40,

789   3479-3483, https://doi.org/10.1002/grl.50650, 2013.

790 Tai, A. P. K., Sadiq, M., Pang, J. Y. S., Yung, D. H. Y., and Feng, Z.: Impacts of Surface Ozone Pollution on Global Crop

791   Yields: Comparing Different Ozone Exposure Metrics and Incorporating Co-effects of CO_2, Frontiers in Sustainable

792   Food Systems, 5, https://doi.org/10.3389/fsufs.2021.534616, 2021.

793 Travis, K. R., Jacob, D. J., Fisher, J. A., Kim, P. S., Marais, E. A., Zhu, L., Yu, K., Miller, C. C., Yantosca, R. M., Sulprizio,

794   M. P., Thompson, A. M., Wennberg, P. O., Crounse, J. D., St. Clair, J. M., Cohen, R. C., Laughner, J. L., Dibb, J. E.,

795   Hall, S. R., Ullmann, K., Wolfe, G. M., Pollack, I. B., Peischl, J., Neuman, J. A., and Zhou, X.: Why do models

796   overestimate surface ozone in the Southeast United States?, Atmos. Chem. Phys., 16, 13561-13577,

797   https://doi.org/10.5194/acp-16-13561-2016, 2016.

798 van der Werf, G. R., Randerson, J. T., Giglio, L., van Leeuwen, T. T., Chen, Y., Rogers, B. M., Mu, M., van Marle, M. J.

799   E., Morton, D. C., Collatz, G. J., Yokelson, R. J., and Kasibhatla, P. S.: Global fire emissions estimates during 1997–

800   2016, Earth Syst. Sci. Data, 9, 697-720, https://doi.org/10.5194/essd-9-697-2017, 2017.

801 Van Dingenen, R., Dentener, F. J., Raes, F., Krol, M. C., Emberson, L., and Cofala, J.: The global impact of ozone on

802   agricultural crop yields under current and future air quality legislation, Atmospheric Environment, 43, 604-618,

803   https://doi.org/10.1016/j.atmosenv.2008.10.033, 2009.

804 Wang, H., Lyu, X., Guo, H., Wang, Y., Zou, S., Ling, Z., Wang, X., Jiang, F., Zeren, Y., Pan, W., Huang, X., and Shen, J.:

805   Ozone pollution around a coastal region of South China Sea: interaction between marine and continental air, Atmos.

806   Chem. Phys., 18, 4277-4295, https://doi.org/10.5194/acp-18-4277-2018, 2018a.

807 Wang, H., Lu, X., Jacob, D. J., Cooper, O. R., Chang, K. L., Li, K., Gao, M., Liu, Y., Sheng, B., Wu, K., Wu, T., Zhang, J.,

808   Sauvage, B., Nédélec, P., Blot, R., and Fan, S.: Global tropospheric ozone trends, attributions, and radiative impacts

809   in 1995–2017: an integrated analysis using aircraft (IAGOS) observations, ozonesonde, and multi-decadal chemical

810   model simulations, Atmos. Chem. Phys., 22, 13753-13782, https://doi.org/10.5194/acp-22-13753-2022, 2022a.

811 Wang, L., Tai, A. P. K., Tam, C.-Y., Sadiq, M., Wang, P., and Cheung, K. K. W.: Impacts of future land use and land cover

812   change on mid-21st-century surface ozone air quality: distinguishing between the biogeophysical and biogeochemical

813   effects, Atmos. Chem. Phys., 20, 11349-11369, https://doi.org/10.5194/acp-20-11349-2020, 2020.

814 Wang, L., Wang, S., Zhou, Y., Liu, W., Hou, Y., Zhu, J., and Wang, F.: Mapping population density in China between 1990

815   and 2010 using remote sensing, Remote Sensing of Environment, 210, 269-281,

816   https://doi.org/10.1016/j.rse.2018.03.007, 2018b.

817 Wang, T., Xue, L., Feng, Z., Dai, J., Zhang, Y., and Tan, Y.: Ground-level ozone pollution in China: a synthesis of recent

818   findings on influencing factors and impacts, Environmental Research Letters, 17, 063003,

819   https://doi.org/10.1088/1748-9326/ac69fe, 2022b.

820 Wang, X., Gong, G., Li, N., and Qiu, S.: Detection Analysis of Epileptic EEG Using a Novel Random Forest Model

821   Combined With Grid Search Optimization, Frontiers in Human Neuroscience, 13,

822   https://doi.org/10.3389/fnhum.2019.00052, 2019.

823 Wang, Y., Zhang, Y., Hao, J., and Luo, M.: Seasonal and spatial variability of surface ozone over China: contributions from

824   background and domestic pollution, Atmos. Chem. Phys., 11, 3511-3525, https://doi.org/10.5194/acp-11-3511-2011,

825   2011.

826 Wang, Y., Wild, O., Ashworth, K., Chen, X., Wu, Q., Qi, Y., and Wang, Z.: Reductions in crop yields across China from

827   elevated ozone, Environmental Pollution, 292, 118218, https://doi.org/10.1016/j.envpol.2021.118218, 2022c.

828 Wei, J., Li, Z., Li, K., Dickerson, R. R., Pinker, R. T., Wang, J., Liu, X., Sun, L., Xue, W., and Cribb, M.: Full-coverage

829   mapping and spatiotemporal variations of ground-level ozone (O_3) pollution from 2013 to 2020 across China, Remote

830   Sensing of Environment, 270, 112775, https://doi.org/10.1016/j.rse.2021.112775, 2022.

831 Wesely, M. L.: Parameterization of surface resistances to gaseous dry deposition in regional-scale numerical models,

832   Atmospheric Environment (1967), 23, 1293-1304, https://doi.org/10.1016/0004-6981(89)90153-4, 1989.

833 Wild, O. and Prather, M. J.: Global tropospheric ozone modeling: Quantifying errors due to grid resolution, Journal of

834   Geophysical Research: Atmospheres, 111, https://doi.org/10.1029/2005JD006605, 2006.

835 Xiao, Q., Chang, H. H., Geng, G., and Liu, Y.: An Ensemble Machine-Learning Model To Predict Historical PM2.5

836   Concentrations in China from Satellite Data, Environmental Science & Technology, 52, 13260-13269,

837   https://doi.org/10.1021/acs.est.8b02917, 2018.

838 Yang, L., Luo, H., Yuan, Z., Zheng, J., Huang, Z., Li, C., Lin, X., Louie, P. K. K., Chen, D., and Bian, Y.: Quantitative

839   impacts of meteorology and precursor emission changes on the long-term trend of ambient ozone over the Pearl River

840   Delta, China, and implications for ozone control strategy, Atmos. Chem. Phys., 19, 12901-12916,

841   https://doi.org/10.5194/acp-19-12901-2019, 2019.

842 Yin, H., Pizzol, M., and Xu, L.: External costs of PM2.5 pollution in Beijing, China: Uncertainty analysis of multiple health

843   impacts and costs, Environmental Pollution, 226, 356-369, https://doi.org/10.1016/j.envpol.2017.02.029, 2017a.

844 Yin, P., Chen, R., Wang, L., Meng, X., Liu, C., Niu, Y., Lin, Z., Liu, Y., Liu, J., Qi, J., You, J., Zhou, M., and Kan, H.:

845   Ambient Ozone Pollution and Daily Mortality: A Nationwide Study in 272 Chinese Cities, Environ Health Perspect,

846   125, 117006, https://doi.org/10.1289/EHP1849, 2017b.

847 Yin, Z. and Ma, X.: Meteorological conditions contributed to changes in dominant patterns of summer ozone pollution in

848   Eastern China, Environmental Research Letters, 15, https://doi.org/10.1088/1748-9326/abc915, 2020.

849 Zhan, Y., Luo, Y., Deng, X., Chen, H., Grieneisen, M. L., Shen, X., Zhu, L., and Zhang, M.: Spatiotemporal prediction of

850   continuous daily PM2.5 concentrations across China using a spatially explicit machine learning algorithm,

851   Atmospheric Environment, 155, 129-139, https://doi.org/10.1016/j.atmosenv.2017.02.023, 2017.

852 Zhang, W., Feng, Z., Wang, X., Liu, X., and Hu, E.: Quantification of ozone exposure- and stomatal uptake-yield response

853   relationships for soybean in Northeast China, Science of The Total Environment, 599-600, 710-720,

854   https://doi.org/10.1016/j.scitotenv.2017.04.231, 2017.

855 Zhang, X., Osei, F., Stein, A., Cheng, C., and Maji, K. J.: Temporal and spatial evolution of short-term exposure to ozone

856   pollution: Its health impacts in China based on a meta-analysis, Journal of Cleaner Production, 373, 133938,

857   https://doi.org/10.1016/j.jclepro.2022.133938, 2022a.

858 Zhang, X., Yan, B., Zhou, Y., Osei, F., Li, Y., Zhao, H., Cheng, C., and Stein, A.: Short-term health impacts related to ozone

859   in China before and after implementation of policy measures: A systematic review and meta-analysis, Science of The

860   Total Environment, 847, 157588, https://doi.org/10.1016/j.scitotenv.2022.157588, 2022b.

861 Zhang, Y., Wang, Y., Gao, M., Ma, Q., Zhao, J., Zhang, R., Wang, Q., and Huang, L.: A Predictive Data Feature Exploration-

862   Based Air Quality Prediction Approach, IEEE Access, 7, 30732-30743,

863   https://doi.org/10.1109/ACCESS.2019.2897754, 2019.

864 Zhang, Z., Yao, M., Wu, W., Zhao, X., and Zhang, J.: Spatiotemporal assessment of health burden and economic losses

865   attributable to short-term exposure to ground-level ozone during 2015-2018 in China, BMC Public Health, 21, 1069,

866   https://doi.org/10.1186/s12889-021-10751-7, 2021.

867 Zhao, Z. and Wang, Y.: Influence of the West Pacific subtropical high on surface ozone daily variability in summertime

868   over eastern China, Atmospheric Environment, 170, 197-204, https://doi.org/10.1016/j.atmosenv.2017.09.024, 2017.

869 Zhou, D., Ding, A., Mao, H., Fu, C., Wang, T., Chan, L. Y., Ding, K., Zhang, Y., Liu, J., Lu, A., and Hao, N.: Impacts of

870   the East Asian monsoon on lower tropospheric ozone over coastal South China, Environmental Research Letters, 8,

871  044011, https://doi.org/10.1088/1748-9326/8/4/044011, 2013.

872